Solar Phys (2010) 264: 189–237
DOI 10.1007/s11207-010-9568-6

Near-Earth Interplanetary Coronal Mass Ejections During Solar Cycle 23 (1996 – 2009): Catalog and Summary of Properties

I.G. Richardson · H.V. Cane

Received: 6 January 2010 / Accepted: 30 April 2010 / Published online: 26 May 2010

Abstract In a previous study (Cane and Richardson, *J. Geophys. Res.* **108**(A4), SSH6-1, 2003), we investigated the occurrence of interplanetary coronal mass ejections in the near-Earth solar wind during 1996 – 2002, corresponding to the increasing and maximum phases of solar cycle 23, and provided a "comprehensive" catalog of these events. In this paper, we present a revised and updated catalog of the ≈300 near-Earth ICMEs in 1996 – 2009, encompassing the complete cycle 23, and summarize their basic properties and geomagnetic effects. In particular, solar wind composition and charge state observations are now considered when identifying the ICMEs. In general, these additional data confirm the earlier identifications based predominantly on other solar wind plasma and magnetic field parameters. However, the boundaries of ICME-like plasma based on charge state/composition data may deviate significantly from those based on conventional plasma/magnetic field parameters. Furthermore, the much studied "magnetic clouds", with flux-rope-like magnetic field configurations, may form just a substructure of the total ICME interval.

Keywords Coronal mass ejections · Interplanetary coronal mass ejections · Interplanetary magnetic field · Magnetic clouds · Solar wind plasma

1. Introduction

Interplanetary coronal mass ejections (ICMEs) are solar wind structures that are generally believed to be the counterparts of coronal mass ejections (CMEs) at the Sun. ICMEs (older

I.G. Richardson (✉) · H.V. Cane
Code 661, NASA/Goddard Space Flight Center, Greenbelt, MD 20771, USA
e-mail: ian.g.richardson@nasa.gov

I.G. Richardson
CRESST and Department of Astronomy, University of Maryland, College Park, MD 20742, USA

H.V. Cane
School of Mathematics and Physics, University of Tasmania, Hobart, Tasmania, Australia
e-mail: hilary.cane@utas.edu.au

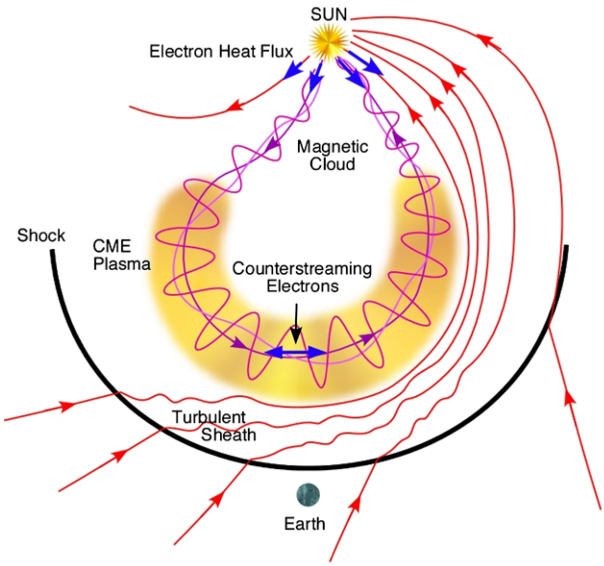

Figure 1 Schematic of an ICME and upstream shock indicating magnetic field, plasma and solar wind suprathermal electron flows (Zurbuchen and Richardson, 2006).

terms include "driver gas", "piston" and "ejecta") are of interest for a number of reasons. For example, ICMEs can drive shocks that accelerate energetic particles (see, *e.g.*, Cane and Lario (2006), Klecker *et al.* (2006), and references therein), are the predominant drivers of intense geomagnetic storms (see, *e.g.*, Zhang *et al.*, 2007; Echer *et al.*, 2008), contain material that has been processed by CME eruptions and provides diagnostic information on conditions during these eruptions (see, *e.g.*, Rakowski, Laming, and Lepri (2007)), modulate the intensity of the galactic cosmic rays (see, *e.g.*, Cane, 2000 and references therein), and can influence the propagation of solar energetic particles in the heliosphere (see, *e.g.*, Richardson and Cane, 1996).

Figure 1 shows a schematic of an ICME driving a shock ahead of it. The shock and ICME are separated by a sheath of compressed, heated, and often turbulent, ambient solar wind plasma. Passage of the ICME may be indicated by various characteristic signatures, as reviewed by Zwickl *et al.* (1983), Gosling (1990, 2000), Neugebauer and Goldstein (1997), and Zurbuchen and Richardson (2006). Some of these signatures are relatively ubiquitous, being observed in most ICMEs, and are therefore particularly useful for the identification of ICMEs. An example is the presence of abnormally low solar wind proton temperatures (Gosling, Pizzo, and Bame, 1973; Richardson and Cane, 1995). Other signatures may be extremely rare. For example, unusually low solar wind ion charge states (*e.g.*, He^+) have only been found in a handful of ICMEs since the beginning of solar wind monitoring (Schwenn, Rosenbauer, and Muehlhaeuser, 1980; Gosling *et al.*, 1980; Zwickl *et al.*, 1982; Yermolaev *et al.*, 1989; Burlaga *et al.*, 1998; Skoug *et al.*, 1999). Figure 1 indicates several representative ICME signatures, in particular a flux-rope-like helical magnetic field configuration that is found in a subset of ICMEs known as "magnetic clouds" (Klein and Burlaga, 1982), bidirectional/counter-streaming solar wind suprathermal electron flows (BDEs) suggestive of looped field lines connected to the hot corona at each footpoint (Gosling *et al.*, 1987a; Gosling, 1990), and plasma properties that differ from those in the ambient solar wind (see, *e.g.*, Richardson and Cane (2004a) and references therein), indicated by the yellow shading.

Because of the interest in ICMEs for a number of fields of study, in Cane and Richardson (2003) we made a "comprehensive" survey of ICMEs in the near-Earth solar wind during

1996 – 2002, encompassing the increasing and maximum phases of solar cycle 23. Some 214 ICMEs were identified, principally on the basis of solar wind plasma and magnetic field signatures, with reference to additional data as available. The associated solar activity (*e.g.*, a CME, flare) was also indicated where this could be identified. This catalog has contributed to over 100 published papers covering the fields of solar, heliospheric, magnetospheric, and ionospheric physics.

In a subsequent study (Richardson and Cane, 2004a), we incorporated solar wind composition and charge state observations made by the Solar Wind Ion Composition Spectrometer (SWICS) instrument (Gloeckler *et al.*, 1998) on the Advance Composition Explorer (ACE) spacecraft into the identification of ICMEs. In particular we discussed the compositional and charge state anomalies found inside the Cane and Richardson (2003) ICMEs and how such anomalies might assist in the routine identification of ICMEs. Solar wind composition and charge states reflect conditions prevailing near the Sun during the acceleration of the solar wind and the formation of ICMEs (see, *e.g.*, Bochsler, 2000; Rakowski, Laming, and Lepri, 2007). In particular, ion charge states "freeze-in" near the Sun because ionization and recombination time-scales become larger than the solar wind ion expansion time as the coronal electron density decreases with increasing distance from the Sun. The ratios of different ionization states then provide information on coronal electron temperatures at the freezing-in altitude (see, *e.g.*, Hundhausen, Gilbert, and Bame, 1968; Owocki, Holzer, and Hundhausen, 1983). For further discussion of SWICS observations within ICMEs; see Lepri *et al.* (2001), Reinard *et al.* (2001), Zurbuchen *et al.* (2003), Richardson *et al.* (2003a), Reisenfeld *et al.* (2003, 2007), Lepri and Zurbuchen (2004), Reinard (2005, 2008).

Motivated by the interest shown in the Cane and Richardson (2003) ICME catalog, in this paper we update the catalog to encompass the full solar cycle 23. In doing so, we have reviewed the earlier identifications of Cane and Richardson (2003) in the light of the SWICS composition and charge state data. We have also considered observations of suprathermal solar wind electron pitch-angle distributions from the SWEPAM instrument on ACE that were not available to us when compiling the Cane and Richardson (2003) catalog. Overall, the vast majority of events in this catalog are also in the revised catalog, as will be discussed further below. Changes are typically in the more marginal events which can be reassessed using the additional data sets. We have also corrected a few typographical errors in the Cane and Richardson (2003) catalog, and have updated the geomagnetic D_{st} values from provisional to final, when available. We plan to continue to update the catalog into cycle 24, and the updated catalog may be obtained from the authors. The catalog is also currently available via the ACE Science Center (http://www.srl.caltech.edu/ACE/ASC/).

Section 2 discusses the instrumentation used to make our ICME identifications and illustrates several examples. Section 3 describes the catalog of ICMEs in 1996 – 2009, while Section 4 summarizes some of the basic properties of these ICMEs including their solar source location, occurrence rate, the fraction of magnetic clouds, transit and *in-situ* speeds, magnetic field intensity, plasma density and proton temperature, ICME and sheath sizes, ICME expansion rate, geomagnetic effects, and plasma composition and charge states. Section 5 discusses the relationship between the magnetic cloud, plasma/field and composition/charge state boundaries. Section 6 compares the catalog with other ICME lists, and Section 7 summarizes the main conclusions of this study.

2. Instrumentation and ICME Identification

We use several data sets to identify potential ICMEs with the philosophy that ideally as many different signatures as possible should be examined when identifying ICMEs. As discussed in greater detail by Cane and Richardson (2003), we examine near-Earth solar wind plasma and magnetic field data from the IMP 8, WIND, and ACE spacecraft and the OMNI near-Earth database at resolutions of ≈1 minute to 1 hour. These data are obtained from the Space Physics Data Facility at the Goddard Space Flight Center (http://spdf.gsfc.nasa.gov/) and the ACE Science Center (http://www.srl.caltech.edu/ACE/ASC/).

In addition we use solar wind ion composition and charge state observations (1- or 2-hour averages) made by the SWICS instrument (Gloeckler *et al.*, 1998) on the ACE spacecraft, launched in August 1997, that were not taken into consideration when compiling the Cane and Richardson (2003) catalog. We discussed the identification of ICMEs using this data set in Richardson and Cane (2004a) and demonstrated that ICMEs tend to be associated with anomalies such as enhanced charge states of oxygen and iron, and increased Mg/O ratios, compared with values in the ambient solar wind (see also Lepri *et al.*, 2001; Reisenfeld *et al.*, 2003; Reinard, 2005, 2008). Since that study, the SWICS data set has been completely revised to include additional ion/charge state measurements, while certain ion ratios (*e.g.*, Mg/O) have been redefined to include a wider range of ion charge states. As a consequence, a few of the conclusions of Richardson and Cane (2004a) using the earlier SWICS database need to be revised (Richardson and Cane, 2010).

Note that we do not use the solar wind He/proton ratio as a *prime* identifier of ICMEs even though it has been well established for many years that some ICMEs are associated with high values of He/p (see, *e.g.*, Hirshberg, Bame, and Robbins, 1972; Borrini *et al.*, 1982). The first reason is that the He/p ratio varies with the level of solar activity. In particular, He/p in slow solar wind increases with solar activity levels (Aellig, Lazarus, and Steinberg, 2001; Richardson *et al.*, 2003b; Richardson and Cane, 2004a; Kasper *et al.*, 2007). Second, there is a large overlap between values of He/p in the ambient solar wind and ICMEs for similar solar wind speeds (Richardson *et al.*, 2003b; Richardson and Cane, 2004a). Third, large values of He/p are only found in a minority of ICMEs. For example He/p > 0.06 is found in ≈30% of the observations in ICMEs discussed by Richardson and Cane (2004a). Thus, it is not possible to state a simple criterion for He/p that differentiates ICMEs from ambient solar wind and identifies a majority of ICMEs.

Another data set not considered by Cane and Richardson (2003) that we have now examined is the ACE/SWEPAM solar wind electron pitch-angle database (http://www.srl.caltech.edu/ACE/ASC/DATA/level3/swepam/). As discussed for example by Gosling *et al.* (1987a) and Gosling (1990), ICMEs may be accompanied by bidirectional suprathermal electron flows, the interpretation being that magnetic field lines in the ICME are looped and rooted in the hot corona at each end. In contrast, unidirectional flows away from the Sun are expected to be observed on open field lines (see Figure 1). In some cases, bidirectional flows are intermittent or absent in ICMEs, suggesting that some or all of the looped field lines may have reconnected with open field lines, possibly via interchange reconnection (see, *e.g.*, Shodhan *et al.*, 2000). We have scanned the 12-hour summary plots of these data for the complete period of the study both to assess whether there are bidirectional flows in our putative ICMEs and to identify other intervals of bidirectional flows that might be indicative of additional ICMEs, to be confirmed by examination of other ICME signatures.

We also refer to energetic particle data from the IMP 8, ACE and SOHO spacecraft. Such data can help to link shocks and ICMEs with specific solar events/CMEs through the intensity-time profiles (see, *e.g.*, Cane, Reames, and von Rosenvinge, 1988; Cane and Lario, 2006) and can also indicate the arrival of ICMEs through the abrupt decrease in intensity that may occur at this time over a wide range of particle energies (keV to GeV (galactic cosmic rays); see, *e.g.*, Sanderson *et al.*, 1990; Cane, 2000). To indicate the galactic cosmic ray (GCR) intensity at Earth, we exploit the high counting rate (hundreds of counts per second) of the anti-coincidence guard of the Goddard Medium Energy (GME) instrument on IMP 8 (McGuire, von Rosenvinge, and McDonald, 1986) that we have used for this purpose in several studies (see, *e.g.*, Cane *et al.* (1994), Richardson, Cane, and Wibberenz (1999), Wibberenz, Richardson, and Cane (2002), Richardson (2004), and references therein). IMP 8 provided observations from 1973 until contact with the spacecraft was lost in October 2006. The GME can also be used to identify the bidirectional field-aligned energetic (≈MeV) ion flows that are often (but not uniquely) associated with the passage of ICMEs (see, *e.g.*, Richardson and Reames, 1993; Richardson, 1994, and references therein). To observe such flows, particle intensities are measured in 8 azimuthal sectors as the spacecraft spins about an axis that is perpendicular to the ecliptic. Because IMP 8 was upstream of the Earth's bow shock for only ≈60% of each ≈13 day geocentric orbit, and data coverage was variable during the period of this study and particularly limited after the official end of the IMP 8 mission in 2001, particle anisotropy data are only available for a subset of the ICMEs in this study. At the time of writing, we do not have such data beyond the end of 2005.

Figure 2 illustrates energetic particle and solar wind magnetic field and plasma data from IMP 8 or ACE for 26 April – 3 May 2001 when various signatures provide evidence for the presence of an ICME following an interplanetary shock on 28 April (green vertical line). The purple vertical lines show our estimates of the ICME boundaries based on plasma and field data. Abnormally low solar wind proton temperatures are indicated by black shading in the T_{p} panel (f) which denotes when $T_{\mathrm{p}} < 0.5T_{\mathrm{exp}}$, where T_{exp} is the "expected" temperature for normally-expanding solar wind with the same speed. T_{exp} is inferred from the V_{sw} vs. T_{p} correlation found in the solar wind outside ICMEs (see Richardson and Cane (1995) for further details) and is over-plotted in red. The ICME leading edge is located at the time when T_{p} falls below T_{exp} while the trailing edge is drawn at the time when T_{p} recovers and the magnetic field direction becomes more variable (panels (d) and (e)) since a reduced level of magnetic field direction variations is one signature of some ICMEs.

Panels (i) to (o) show solar wind composition and charge state observations, in particular SWICS measurements of O^7/O^6, mean Fe charge ($\langle Q_{\mathrm{Fe}}\rangle$), and Fe/O together with three color panels ((l) to (n)) indicating the fraction of the observed oxygen, silicon and iron ions that have particular charge states for each 2-hour averaging period. The He/proton ratio from ACE/SWEPAM is shown in panel (o). Note that O^7/O^6, $\langle Q_{\mathrm{Fe}}\rangle$, Fe/O and He/p are all elevated inside the ICME. (The expected value for O^7/O^6, based on variations of this ratio with solar wind speed in normal (non-ICME) solar wind (see Richardson and Cane (2004a) for further details), is overlaid in red in panel (i).) The charge state distributions also show increases in the most prominent charge states of oxygen, silicon and iron that commence close to the time of the ICME leading edge inferred from the plasma/field data. On the other hand, the ion charge states return to ambient solar wind values well after the inferred ICME trailing edge, at the time of the solid vertical blue line for iron and at the dashed blue line, ≈32 hours after the suggested ICME trailing edge, for oxygen and silicon. The He/p ratio also finally declines at this time. Thus, while the composition/charge state data tend to confirm the ICME leading edge inferred from plasma/field data (there is a He/p data gap at this time, however), they suggest that ICME-like plasma with high charge states indicative of strong heating near the Sun (coronal temperatures $\approx 2 - 3 \times 10^6$ K) that was also enriched in Fe and He extended well beyond the inferred ICME trailing edge, in a region with only slightly lower than expected proton temperatures. Overall, the nearly 4 day interval extending from the leading edge of the ICME to the end of the charge state/compositional anomalies corresponds to a radial distance of ≈1 AU when taking the solar wind speed into account.

Turning to energetic particle observations, the time of the solar particle event onset (panel (b)) is consistent with the shock and ICME being associated with the 1006 km s^{-1} halo CME

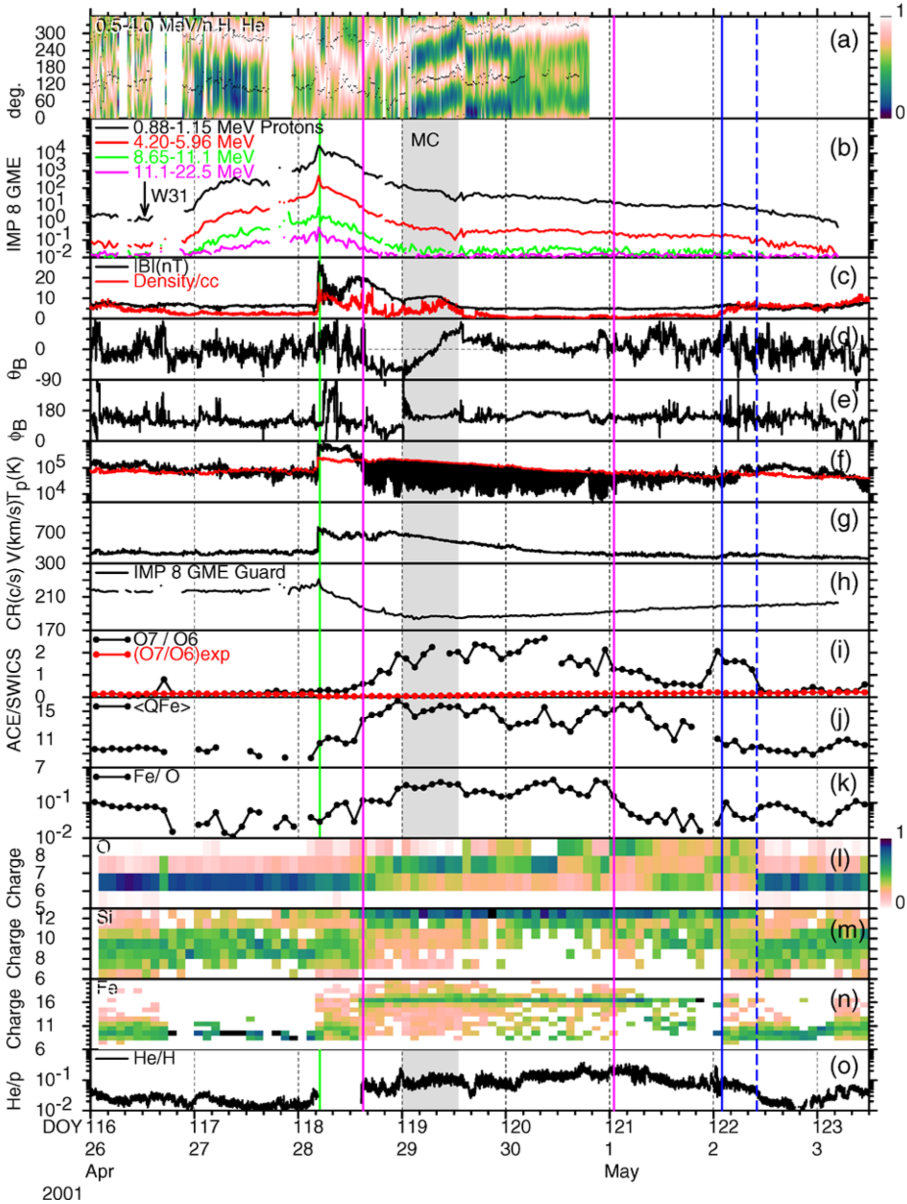

Figure 2 Example of an ICME, in April – May, 2001, accompanied by various signatures in: IMP 8 GME energetic particle data ((a) 0.5 – 4 MeV proton angular distributions, (b) 0.88 – 22 MeV proton intensities and (h) anti-coincidence guard count rate); ACE solar wind magnetic field data ((c) intensity, (d) polar angle, (e) azimuthal angle, in GSE coordinates); ACE solar wind plasma data ((c) density, (f) proton temperature with the expected temperature shown in red, (g) speed, and (o) He/proton ratio); and ACE solar wind composition/charge state data ((i) O^7/O^6 and expected value (red), (j) mean Fe charge state, (k) Fe/O ratio, fractional charge states for (l) O, (m) Si and (n) Fe). Vertical lines indicate: (green) passage of an interplanetary shock, (purple) ICME boundaries inferred from plasma and field data, (solid blue) the trailing edge of the region of enhanced Fe charge states, and (dashed blue) the trailing edge of the region of enhanced O and Si charge states. Note that the reported magnetic cloud (Huttunen *et al.*, 2005) shaded gray is only a substructure of the region of ICME-like plasma.

at 1230 UT on 26 April observed by the LASCO coronagraphs on the SOHO spacecraft and related to a 2B/M7.8 flare at N17°W31°. This implies a 1 AU transit speed for the shock of 1040 $\mathrm{km\,s^{-1}}$ which is reasonably consistent with the CME expansion speed (which will suffer from plane of the sky projection effects) and solar wind speeds of $\leq$730 $\mathrm{km\,s^{-1}}$ following the shock. The typical cosmic ray depression commencing at the shock is evident in the counting rate of the anti-coincidence guard of GME in panel (h). There is often a "second step" at ICME entry (see, *e.g.*, Cane *et al.*, 1994; Cane, 2000), but such a feature is not evident in this event. Panel (a) shows 0.5 – 4 MeV proton anisotropies in the solar wind frame measured by this instrument. The particle intensities in the 8 azimuthal sectors are first smoothed by fitting to a third-order Fourier series in azimuth. The resulting intensity is then normalized to the maximum value in each 15-minute interval and plotted vs. viewing direction (in GSE coordinates) such that particles arriving from the direction of the Sun (or an approaching shock) along the Parker spiral field ($\approx$315°) have higher intensities towards the top of the panel while sunward-flowing particles ($\approx$135°) lie below center. Black dashes are aligned with or opposite to the local magnetic field direction. In addition to the typical flow reversal, from anti-solar to sunward, close to shock passage in the particle enhancement peaking at shock passage, bidirectional field-aligned particle flows can clearly be identified within the ICME, extending to the end of the available observations shortly before passage of the ICME trailing edge.

Solar wind electron data from ACE/SWEPAM are not included in Figure 2. However, examination of the on-line pitch-angle distributions suggests that bidirectional flows were observed from around midday on 28 April, consistent with the leading edge of the ICME, and may have extended until late on 1 May, consistent with the ICME trailing edge, though with a stronger flow in the anti-solar direction.

The gray shaded interval in Figure 2 indicates the magnetic cloud identified by Huttunen *et al.* (2005) and also included on the WIND magnetic cloud list compiled by R.P. Lepping (http://lepmfi.gsfc.nasa.gov/mfi/mag_cloud_S1.html). Note that the magnetic cloud is only a small substructure of the region in which other ICME signatures are observed. Thus, the observations are not consistent with Figure 1 where ICME-like plasma is confined to the flux-rope-like structure. Furthermore, there is little to distinguish the magnetic cloud interval in parameters shown in Figure 2 other than the magnetic field.

A further interesting feature is the quiet, near-radial magnetic field following the magnetic cloud. Similar intervals of quiet radial fields in the trailing edges of some ICMEs were discussed by Neugebauer, Goldstein, and Goldstein (1997) who suggested that they were flows from transient coronal holes opened during the eruption of coronal mass ejections. Another possibility is that the Earth remained inside the "leg" of the ICME during this period. Below we will summarize the relationship between magnetic cloud intervals and other ICME signatures which may help to indicate the origin of the mismatch between the magnetic cloud and ICME boundaries in such events.

Figure 3 shows similar observations for a contrasting ICME in which the ICME boundaries (purple vertical lines) inferred from plasma and magnetic field data are essentially co-located with enhancements in oxygen and iron charge states (corresponding coronal temperatures $\approx 2 \times 10^6$ K), the WIND magnetic cloud region (gray shading) and bidirectional solar wind electron flows observed by ACE/SWEPAM (not shown here). Hence the observations are more consistent with the configuration in Figure 1. The ICME/magnetic cloud here is followed by a corotating high-speed solar wind stream. Note also that there is no increase in Fe/O (panel (k)) inside this ICME. There are no IMP 8 energetic particle anisotropy data for much of the interval shown.

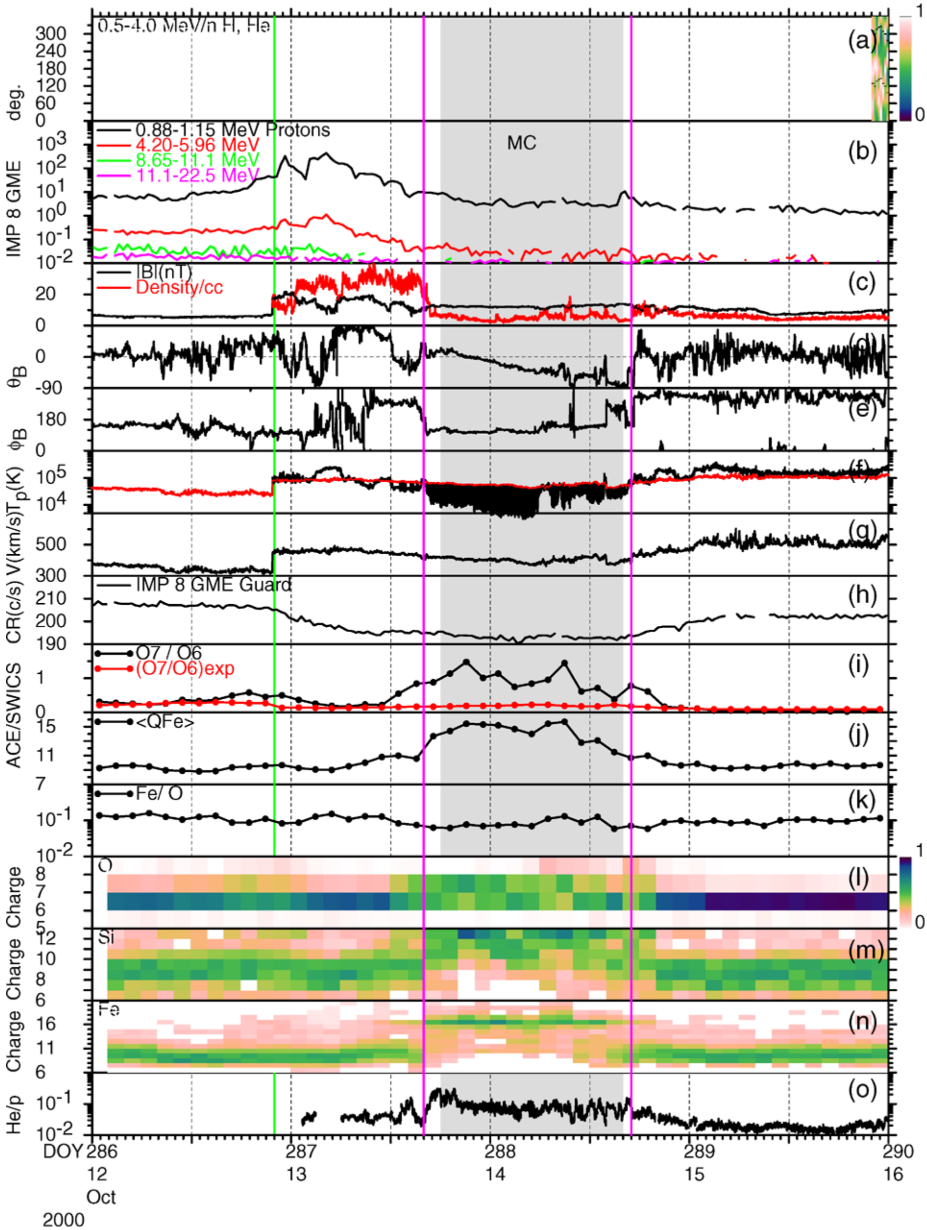

Figure 3 Example of an ICME, in October 2000 (in the format of Figure 2), where the plasma, field and composition/charge state signatures, and reported magnetic cloud (gray shading) are approximately co-located. There are no IMP 8 GME ion distributions (panel (a)) for most of this interval.

Figure 4 shows another representative event, in this case an ICME that lacks a magnetic cloud structure. Rather, the field direction (panels (d) and (e)) is fluctuating, with several discontinuities. As noted by Cane and Richardson (2003) and other studies (see, *e.g.*, Gosling (1990), Richardson and Cane (2004b), and references therein), a majority of ICMEs ob-

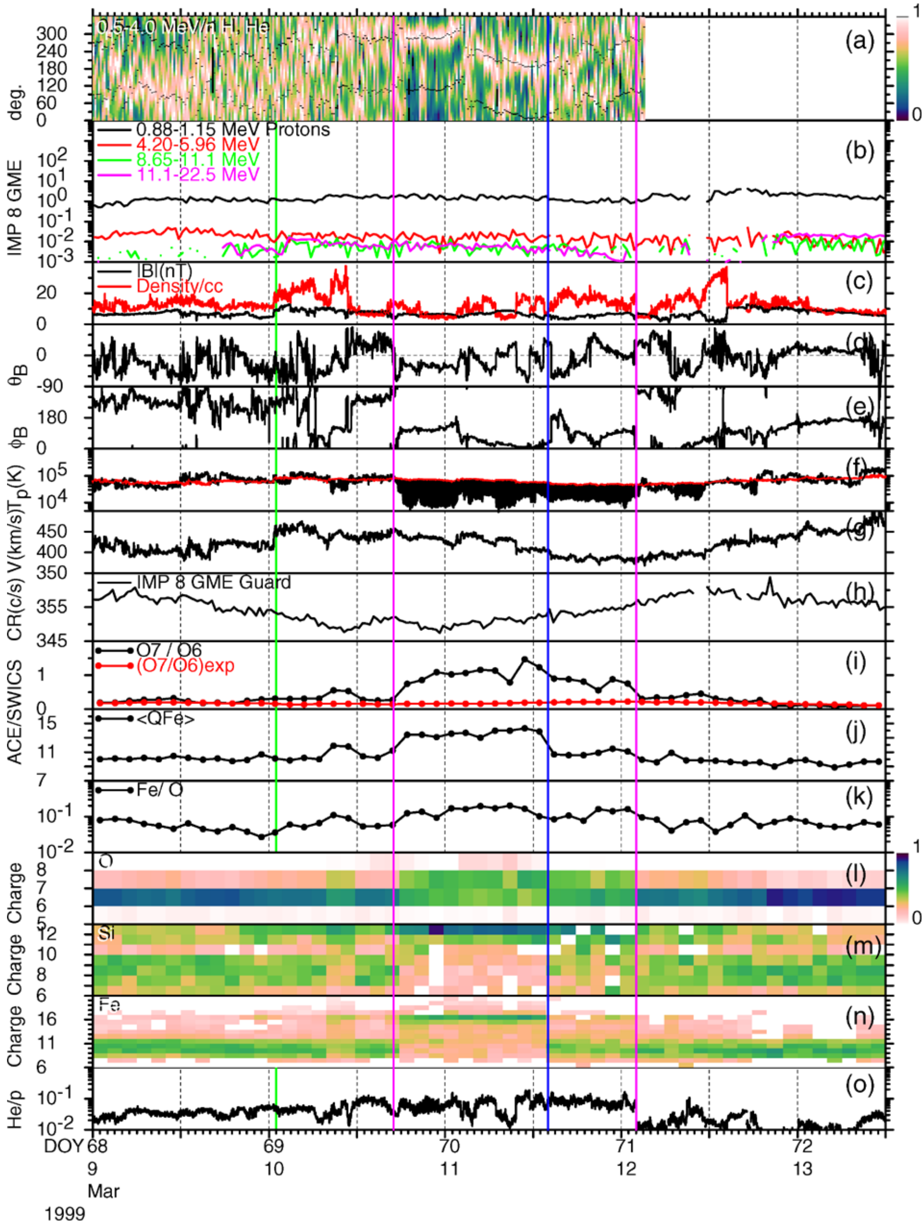

Figure 4 Example of an ICME, in March 1999 (in the format of Figure 2), that lacks a magnetic cloud signature and includes a magnetic field that is variable in strength and direction. Otherwise, the plasma and composition/charge state signatures are similar to those in the ICMEs illustrated in previous figures. The blue vertical line indicates the end of the interval of enhanced Fe charge states.

served at Earth do not include a magnetic cloud, as will be discussed further below. This ICME followed a weak shock (green vertical line) on 10 March 1999. The ICME interval (bounded by purple vertical lines) is based predominantly on the most prominent region of low proton temperatures (panel (f)). Enhanced oxygen charge states (coronal temperatures $\approx 2 \times 10^6$ K) occupy essentially the same region (panels (i) and (l)) while enhanced Fe charge states (panels (j) and (n)) are only observed until $\approx$12 hours before the ICME trailing edge (blue vertical line). Energetic ion intensities (panel (b)) are lower than in Figure 3 and particle flows (panel (a)) are less distinct. However, the particles evidently became more "beamed" along the magnetic field inside the ICME, and though flow anti-parallel to the magnetic field direction is predominant, there are indications of intermittent bidirectional flows (as was also the case for suprathermal electrons; Zurbuchen and Richardson, 2006). Note also that except for the magnetic field, the observations in Figure 4 are quite similar to those in Figure 3.

3. ICMEs in 1996 – 2009

Using observations such as described in the previous section, we have identified some 322 probable ICMEs that passed Earth during 1996 – 2009, listed in Tables 1, 2, 3, 4, 5, 6, 7, 8, 9, 10, 11, and 12. Column 1 in each table gives the start time of the ICME-related "disturbance". For a fast ICME, this is given by the arrival of the ICME-driven shock. In this case, the time given is typically that of the geomagnetic storm sudden commencement (SC) that frequently accompanies a shock reaching the Earth's magnetosphere since this provides a spacecraft-independent arrival time that is also appropriate for comparison with phenomena at the Earth. If an SC is not reported, we give the time of shock passage at ACE (indicated by (A)). If there are no data at ACE, or a shock is not reported at that spacecraft, the shock time at WIND (W) is listed if a shock is reported. We have referred to the ACE shock list (http://www.ssg.sr.unh.edu/mag/ace/ACElists/obs_list.html#shocks) and the shock database compiled by Justin Kasper (Harvard-Smithsonian Center for Astrophysics; http://www.cfa.harvard.edu/shocks/). If no shock is reported for a slower ICME, a wave-like feature or developing shock may be evident in the plasma and field data. The time of such a feature is given in the table to the nearest hour.

If no upstream disturbance is evident, for example in the case of an ICME that has a similar speed to the ambient solar wind, then the disturbance time listed corresponds to the start time of the ICME, also shown in Column 2. Column 3 shows the ICME end time. The ICME start and end times are inferred, as in Cane and Richardson (2003), primarily from plasma and magnetic field data (examples are bounded by the purple lines in Figures 2 – 4) and given to the nearest hour. Columns 4 and 5 show the estimated offsets ($t_{\mathrm{comp}} - t_{\mathrm{ICME}}$, in hours) of the start and end times of the compositional/charge state signatures in the vicinity of the ICME relative to the "ICME" start and end times in Columns 2 and 3 respectively. Here, "ns" indicates that there is no compositional/charge state signature while "nc" indicates that there is no change or there is no clear compositional/charge state change. An absence of data is indicated by "...". Close agreement between the ICME and composition/charge state boundaries (to within an hour or so, limited by the resolution of the SWICS data) is indicated by a "zero hour" offset. As noted above, different compositional/charge state changes may not coincide exactly though frequently there is a consensus. We typically use the O^7/O^6 ratio as a reference.

Columns 6 and 7 give the offsets (in hours) of the magnetic cloud leading and trailing boundaries relative to the ICME boundaries ($t_{\mathrm{mc}} - t_{\mathrm{ICME}}$), based primarily on the WIND magnetic cloud list. Additional events identified by Huttunen *et al.* (2005) in 1996 – 2003 are also included. Occasionally, two magnetic clouds are identified in the interval of interest, indicated by "(2)". The offsets are then estimated from the leading edge of the first magnetic cloud and the trailing edge of the second.

Table 1 Near-Earth ICMEs in 1996 – 1997.

Column 1 Disturbance mon/day UT	2 ICME Start mon/day UT	3 ICME End mon/day UT	4 Start C	5 End C	6 Start MC	7 End MC	8 BDE	9 BIF	10 Qual.	11 ΔV ($km\,s^{-1}$)	12 V_I ($km\,s^{-1}$)	13 V_{max} ($km\,s^{-1}$)	14 B (nT)	15 MC?	16 D_{st} (nT)	17 V_{tr} ($km\,s^{-1}$)	18 LASCO CME mon/day UT
1996																	
05/27 1500	05/27 1500	05/29 0300	…	…	0	+4	N	…	2	0	370	400	9	2	−33	…	
07/01 1320	07/01 1800	07/02 1100	…	…	0	0	N	…	3	40	360	370	11	2	−20	…	
08/07 0600	08/07 1200	08/08 1000	…	…	0	0	N	…	2	10	350	380	7	2	−23	…	
12/23 1600	12/23 1700	12/25 1100	…	…	+10	0	N	…	2	20	360	420	10	2	−18	435	12/19 1630 H
1997																	
01/10 0104	01/10 0400	01/11 0200	…	…	0	0	Y	…	1	100 S	450	460	14	2	−78	507	01/06 1510 H
02/09 1321	02/10 0200	02/10 1900	…	…	0	0	Y	…	2	90 S	450	600	8	2	−68	683	02/07 0030 H
04/10 1745	04/11 0600	04/11 1900	…	…	0	0	Y	…	1	150	460	470	20	2	−82	552	04/07 1427 H
04/21 0600	04/21 1000	04/23 0400	…	…	+4	+2	Y	…	2	40	360	420	12	2	−107	…	
05/15 0159	05/15 0900	05/16 0000	…	…	0	0	N	Y	1	150 S	450	480	21	2	−115	616	05/12 0530 H
05/26 0957	05/26 1600	05/27 1000	…	…	0	+9	Y	…	2	70 S	340	350	10	2H	−74	381	05/21 2100
06/08 1636	06/08 1800	06/10 0000	…	…	+8	0	Y	…	3	30	380	400	12	2	−84	…	
06/19 0032	06/19 0600	06/20 2300	…	…	0	−31	Y	Y	2	60	360	390	8	2	−36	…	
07/15 0311	07/15 0800	07/16 1100	…	…	0	−11	Y	Y	2	80	350	360	10	2	−45	…	
08/03 1042	08/03 1300	08/04 0300	…	…	0	0	Y	…	1	80	400	480	16	2	−48	410	07/30 0445 H
08/17 0200	08/17 0600	08/17 2000	…	…	…	…	N	…	2W	60	390	410	7	0	−28	…	
09/03 0800	09/03 1300	09/03 2100	…	…	…	…	Y	N	3W	40 S	410	430	14	1	−98	405	08/30 0130 H
09/21 1651	09/21 2100	09/22 1600	…	…	+3	0	N	…	1	110	440	470	16	2	−36	450	09/17 2028 H
10/01 0059	10/01 1600	10/02 2300	…	…	0	0	Y	N	1	60 S	450	470	10	2	−98	580	09/28 0108 H
10/10 0300	10/10 1100	10/10 2200	…	…	…	…	Y	…	2	30	430	460	8	1	−64	…	
10/10 1612	10/10 2200	10/12 0000	…	…	0	0	Y	Y	1	40 S	400	450	12	2	−130	430	10/06 1528
10/26 1200	10/27 0000	10/28 0700	…	…	…	…	Y	…	2	40	500	520	7	1	−60	572	10/23 1126 H

Table 1 (*Continued*)

Column 1	2	3	4	5	6	7	8	9	10	11	12	13	14	15	16	17	18
Disturbance mon/day UT	ICME Start mon/day UT	ICME End mon/day UT	Start C	End C	Start MC	End MC	BDE	BIF	Qual.	ΔV (km s^{-1})	V_I (km s^{-1})	V_{max} (km s^{-1})	B (nT)	MC?	D_{st} (nT)	V_{tr} (km s^{-1})	LASCO CME mon/day UT
11/06 2248	11/07 0400	11/09 1200	…	…	+11	−21(2)	Y	N	2	140 S	400	460	11	2	−110	640	11/04 0610 H
11/22 0949	11/22 1900	11/23 1400	…	…	0	−2	Y	…	1	170 S	510	520	17	2	−108	640	dg(11/19 1700)
11/23 1900	11/24 0000	11/25 0000	…	…	…	…	Y	…	2	100	530	590	5	0	−47	…	
12/10 0526	12/10 1800	12/12 0000	…	…	…	…	…	…	2	50 S	350	380	12	0	−60	460	12/06 1027
12/30 0209	12/30 1000	12/31 1100	…	…	…	…	Y	…	3	50 S	370	410	12	1	−77	430	12/26 0231

Column: (1) Disturbance arrival time – shock/bow wave if present (SC time, or at ACE (A) or WIND (W)), otherwise ICME leading edge; (2) ICME start time; (3) ICME end time; (4) and (5) Offsets of start and end of compositional/charge state signature with respect to ICME times; (6) and (7) Offsets of start and end of magnetic cloud with respect to ICME times; (8) Bidirectional suprathermal electron flows in ICME (yes/no); (9) Bidirectional energetic (≈1 MeV) ion flows in ICME based on IMP 8 GME data; (10) Quality of ICME boundary time estimates (1 = best); (11) Increase in solar wind speed at disturbance. 'S' indicates this included a shock; (12) Mean solar wind speed in ICME interval; (13) Maximum solar wind speed in interval from disturbance to ICME trailing edge; (14) Mean magnetic field intensity in ICME interval; (15) 2 = reported magnetic cloud, 1 = evidence of magnetic field rotation, but ICME does not meet magnetic cloud criteria; 0 = no magnetic cloud-like features. 'H' indicates MC is from Huttunen *et al.* (2005); (16) Minimum value of geomagnetic D_{st} index; (17) 1 AU transit speed of disturbance based on (18) Time of associated solar event, generally given by the time of the CME ('H' = halo CME) observed by SOHO/LASCO. 'dg' indicates that a LASCO data gap encompassed the likely solar event time. In some such cases, the time of the related flare is given in brackets. Major changes from Cane and Richardson (2003): 1996, 08/07 Disturbance changed to 0600; 1997 02/16 Removed; 1997 05/26 Changed to magnetic cloud (Huttunen *et al.*, 2005); 1997 09/17 Removed; 1997 10/10 0300 Added; 1997 11/06 D_{st} corrected, from −11 to −110 nT.

Table 2 Near-Earth ICMEs in 1998.

Column 1 Disturbance mon/day UT	2 ICME Start mon/day UT	3 ICME End mon/day UT	4 Start C	5 End C	6 Start MC	7 End MC	8 BDE	9 BIF	10 Qual.	11 ΔV ($\mathrm{km\,s^{-1}}$)	12 V_{I} ($\mathrm{km\,s^{-1}}$)	13 $V_{\max}$ ($\mathrm{km\,s^{-1}}$)	14 B (nT)	15 MC?	16 D_{st} (nT)	17 V_{tr} ($\mathrm{km\,s^{-1}}$)	18 LASCO CME mon/day UT
1998																	
01/06 1416	01/07 0100	01/08 2200	…	…	+2	0(2)	Y	..	2	80 S	400	410	16	2	−77	480	01/02 2328 H
01/09 0700	01/09 0700	01/10 0800	…	…	…	…	N	…	2	0	450	500	6	1	−28	…	
01/20 0000	01/20 1700	01/21 0400	…	…	…	…	Y	…	3W	50	430	450	5	1	−29	…	
01/21 0400	01/21 0600	01/22 1300	…	…	…	…	N	…	3W	0	380	400	13	0	−11	430	01/17 0409 H
01/28 1600(A)	01/29 2000	01/31 0100	…	…	…	…	Y	N	2	30 S	380	410	7	0	−55	557	01/25 1526 H
02/04 0000	02/04 0400	02/05 2300	…	…	0	0	Y	…	1	50	320	390	11	2	−34	…	
02/17 0400	02/17 1000	02/17 2100	ns	ns	0	+7	Y	…	2W	30	400	420	12	2H	−100	602	02/14 0655
02/18 0750(A)	02/19 0100	02/20 0000	−3	…	…	…	N	…	2	20 S	440	460	9	1	−51	…	
03/04 1156	03/04 1300	03/06 0900	0	−9	0	−3	N	…	1	30 S	350	380	12	2	−36	440	02/28 1248
03/25 1000	03/25 1300	03/26 1000	…	…	…	…	Y	Y	1	20	400	400	10	1	−56	…	
03/30 2200	03/31 1100	04/03 0200	−6	0	…	…	N	Y	1	30	360	430	7	0	−35	…	
04/11 2300	04/11 2300	04/13 1800	ns	ns	…	…	N	…	3W	20	390	390	8	0	−46	…	
05/01 2156	05/02 0500	05/04 0200	−2	−24	+7	−9	Y	Y	1	150 S	520	650	11	2	−85	780	04/29 1658 H
05/04 0215(A)	05/04 1000	05/07 2300	−7	0	…	…	Y	…	2	250	550	780	10	0	−205	1150	05/02 1406 H
06/02 0800	06/02 1000	06/02 1800	…	…	0	0	N	…	2	10	390	400	9	2	−1	…	
06/13 1925	06/14 0400	06/15 0600	…	…	…	…	Y	N	3	80 S	340	380	10	1	−55	…	
06/24 1000	06/24 1600	06/25 2300	0	0	0	0	Y	…	2	80	450	540	12	2	−25	…	06/21 0535?
06/25 1636	06/26 0400	06/26 1900	0	0	…	…	Y	…	2	30 S	470	490	11	0	−101	…	
07/05 0315(A)	07/06 0600	07/09 0700	0	…	…	…	N	…	1	50 S	450	630	5	0	−30	dg	dg
07/10 2300	07/11 0000	07/13 1500	…	…	…	…	Y	Y	3W	20	400	430	10	0	−35	dg	dg
08/01 0400	08/01 0400	08/03 1000	0	…	…	…	N	Y	3	30	410	450	7	1	−6	dg	dg
08/05 1300	08/05 1300	08/06 1200	…	…	…	…	Y	Y	2W	0	360	390	8	1	−138	dg	dg

Table 2 (*Continued*)

Column 1 Disturbance mon/day UT	2 ICME Start mon/day UT	3 ICME End mon/day UT	4 Start C	5 End C	6 Start MC	7 End MC	8 BDE	9 BIF	10 Qual.	11 ΔV ($\mathrm{km\,s^{-1}}$)	12 V_I ($\mathrm{km\,s^{-1}}$)	13 V_{max} ($\mathrm{km\,s^{-1}}$)	14 B (nT)	15 MC?	16 D_{st} (nT)	17 V_{tr} ($\mathrm{km\,s^{-1}}$)	18 LASCO CME mon/day UT
08/07 1100	08/07 2300	08/09 2300	...	...	...	...	N	Y	2	0	450	500	7	0	−62	dg	dg
08/10 0046	08/10 1100	08/10 2200	ns	ns	...	...	Y	N	3W	100 S	450	500	7	0	−27	dg	dg
08/11 2300	08/12 0100	08/13 1400	ns	ns	...	...	Y	...	3W	20	370	420	8	1	−19	dg	dg
08/19 1847	08/20 0600	08/21 2000	0	0	+4	0	Y	Y	1	50 S	320	340	13	2	−67	dg	dg
08/26 0651	08/26 2200	08/28 0000	0	+18	...	...	Y	...	2	200 S	650	860	14	0	−155	1260	dg (08/24 2200)
09/23 0200	09/23 0400	09/23 1800	ns	ns	...	...	Y	N	2	80	420	490	7	1	−33	dg	dg
09/24 2345	09/25 0600	09/26 1600	−2	+4	+4	−3	Y	Y	1	300 S	640	770	13	2	−207	1020	dg (09/23 0700)
10/18 1952	10/19 0400	10/20 0700	0	0	0	−17	Y	Y	1	50 S	390	430	18	2	−112	510	10/15 1004 H
10/23 1230(A)	10/23 1500	10/24 1600	0	0	...	...	N	Y	3	50 S	520	600	7	0	−52	...	
11/07 0815	11/07 2200	11/09 0100	0	0	...	...	Y	...	2	130 S	450	530	15	1	−81	570	11/04 0754 H
11/08 0451	11/09 0100	11/11 0100	+8	+17	0	−24	Y	...	2	200 S	450	640	12	2	−149	740	11/05 2044 H
11/13 0143	11/13 0200	11/14 1200	ns	ns	0	−6	Y	N	3	50	390	400	17	2H	−131	520	11/09 1818
11/30 0507	11/30 2100	12/01 0400	0	0	...	...	Y	...	2	100 S	470	480	9	0	−15	...	
12/28 1826	12/29 1800	12/31 0200	0	0	...	...	N	...	2	30 S	400	410	8	0	−58	dg	dg

Major changes from Cane and Richardson (2003): D_{st} updated to final for all events; 01/28 Disturbance time changed from 01/29 1800 to 01/28 1600; 02/17 Changed to magnetic cloud (Huttunen *et al.*, 2005); 03/06 Removed; 03/25 Removed; 03/30 Added; 05/15 Removed; 05/29 Removed; 07/30 Removed; 08/07 Disturbance time changed to 1300; 11/08 ICME times revised; 11/12 Disturbance time corrected to 11/13 0143 UT, changed to magnetic cloud (Huttunen *et al.*, 2005); 11/30 ICME times revised.

Table 3 Near-Earth ICMEs in 1999.

Column 1 Disturbance mon/day UT	2 ICME Start mon/day UT	3 ICME End mon/day UT	4 Start C	5 End C	6 Start MC	7 End MC	8 BDE	9 BIF	10 Qual.	11 ΔV ($km\,s^{-1}$)	12 V_I ($km\,s^{-1}$)	13 V_{max} ($km\,s^{-1}$)	14 B (nT)	15 MC?	16 D_{st} (nT)	17 V_{tr} ($km\,s^{-1}$)	18 LASCO CME mon/day UT
1999																	
01/04 0000	01/04 0400	01/04 2200	ns	ns	…	…	Y	…	3W	20	350	360	8	0	−29	dg	dg
01/13 1054	01/13 1500	01/13 2300	0	0	…	…	N	…	2	70 S	420	430	18	0	−112	dg	dg
01/22 1950(A)	01/23 0900	01/23 1800	nc	0	…	…	Y	…	3	120 S	570	660	12	0	−52	dg	dg
02/13 1900	02/13 1900	02/14 1500	0	−3	…	…	N	…	3W	20	440	470	9	0	−17	…	
02/16 1500	02/16 1500	02/17 1100	0	0	…	…	N	…	3	0	460	470	6	1	−7	…	
02/17 0709	02/17 1600	02/18 1000	0	0	…	…	Y	…	3	30 S	410	490	8	0	−34	…	
02/18 0246	02/18 1000	02/20 1700	0	0	+4	−29	Y	…	2	250 S	540	700	9	2	−123	870	dg (02/16 0312)
03/10 0130	03/10 1700	03/12 0200	0	0	…	…	Y	Y	2	30 S	410	460	7	0	−81	…	
03/19 1000	03/19 1100	03/20 1200	0	0	…	…	Y	…	3W	10	340	380	5	1	−30	…	
04/16 1125	04/16 1800	04/17 1900	−6	+8	+2	+2	Y	…	1	50 S	410	460	18	2	−91	520	04/13 0330 H
04/20 1600	04/21 0400	04/22 1400	0	+10	+8	0	Y	…	1	120	490	620	8	2H	−29	…	04/18 0830?
05/15 1600	05/15 1600	05/18 0000	ns	0	…	…	N	…	3	0	390	400	5	0	−13	…	
06/02 2000	06/02 2300	06/03 2200	nc	0	…	…	Y	Y	3	40	430	470	9	1	−6	…	
06/26 2016	06/27 2200	06/29 0400	0	…	…	…	Y	Y	3	100 S	670	860	7	0	−41	760	06/24 1331 H
07/02 0059	07/03 0500	07/06 0600	−26	ns	…	…	…	…	2	100 S	440	680	4	0	−26	…	
07/06 1509	07/06 2100	07/07 0200	ns	…	…	…	N	…	2	50 S	460	500	10	1	−4	620	07/03 1954
07/07 0600	07/07 0700	07/08 0400	nc	nc	…	…	Y	…	3	70	450	480	4	0	−1	…	
07/26 2333(A)	07/27 1700	07/29 1200	+26	+2	…	…	Y	…	3	30 S	390	460	6	0	−38	560	07/23 2130
07/30 1600	07/30 2000	07/31 0800	0	0	…	…	Y	…	3	90	620	660	9	0	−52	710	07/28 0530? H
07/31 1837	07/31 1900	08/02 0600	0	ns	…	…	N	…	3	100	480	650	5	1	−39	510	07/28 0906 H
08/02 1100	08/02 1500	08/03 1500	+2	+6	…	…	N	Y	3	20	370	440	4	0	−16	…	
08/08 1841	08/08 2000	08/10 1700	0	0	+25	0	Y	Y	2	20 S	360	410	9	2	−47	…	

Table 3 (*Continued*)

Column 1 Disturbance mon/day UT	2 ICME Start mon/day UT	3 ICME End mon/day UT	4 Start C	5 End C	6 Start MC	7 End MC	8 BDE	9 BIF	10 Qual.	11 ΔV (km s^{-1})	12 V_I (km s^{-1})	13 V_{max} (km s^{-1})	14 B (nT)	15 MC?	16 D_{st} (nT)	17 V_{tr} (km s^{-1})	18 LASCO CME mon/day UT
08/11 2300	08/12 0300	08/14 0000	+16	0	...	...	Y	...	3	40	380	420	6	0	−13	615	08/09 0326
08/20 2300	08/20 2300	08/23 1100	+31	+6	...	...	Y	...	2	0	460	570	7	1	−66	510	08/17 1331
09/21 1200	09/21 1200	09/22 1200	−3	−4	+9	−7	Y	N	3	0	360	380	9	2	−41	...	
09/22 1222	09/22 1900	09/24 0300	0	0	...	...	Y	Y	1	120 S	530	600	11	0	−173	770	09/20 0606 H
10/21 0225	10/21 0800	10/22 0700	+14	0	...	...	Y	N	2	30 S	480	550	20	0	−237	561	10/18 0006 H
11/11 1900	11/12 1000	11/13 1800	−10	nc	...	...	N	...	2	50	450	680	5	0	−69	dg	dg
11/13 1200	11/13 2000	11/15 0000	nc	nc	+4	−15	N	...	3W	50 S	440	480	7	2H	−106	dg	dg
11/22 0000	11/22 0000	11/24 0300	−8	+6	...	...	Y	...	3	40	450	490	9	0	−41	dg	dg
12/12 1551	12/12 1900	12/13 1600	...	0	...	...	Y	Y	2	300 S	520	700	12	0	−85	dg	dg
12/13 2300	12/14 0400	12/14 2000	...	...	...	...	Y	...	2	20	440	480	12	0	−33	dg	dg
12/26 2130(A)	12/27 1100	12/28 0400	−9	+23	...	...	Y	...	3	50 S	430	450	8	1	−8	...	

Major changes from Cane and Richardson (2003): D_{st} updated to final for all events; 02/17 Added; 03/10 ICME trailing edge revised; 03/19 Added; 04/20 Changed to magnetic cloud (Huttunen *et al.*, 2005); 06/26 0325 Removed; 06/26 1216 ICME boundaries revised; 07/02 ICME leading edge revised; 07/06 Divided into two events; 07/07 Added; 08/11 ICME leading edge revised; 08/20 ICME trailing edge revised; 09/21 Added; 09/22 ICME trailing edge revised; 10/21 Transit speed corrected; 11/13 Added.

Table 4 Near-Earth ICMEs in 2000, January–June.

Column 1 Disturbance mon/day UT	2 ICME Start mon/day UT	3 ICME End mon/day UT	4 Start C	5 End C	6 Start MC	7 End MC	8 BDE	9 BIF	10 Qual.	11 ΔV ($\mathrm{km\,s^{-1}}$)	12 V_{I} ($\mathrm{km\,s^{-1}}$)	13 $V_{\max}$ ($\mathrm{km\,s^{-1}}$)	14 B (nT)	15 MC?	16 D_{st} (nT)	17 V_{tr} ($\mathrm{km\,s^{-1}}$)	18 LASCO CME mon/day UT
2000																	
01/22 0023(A)	01/22 1700	01/23 0200	0	0	…	…	Y	…	2	30 S	380	400	16	1	−97	530	01/18 1754 H
02/11 0258	02/11 1600	02/11 2000	0	0	…	…	Y	N	1	60 S	420	510	7	0	−25	630	02/08 0930 H
02/11 2352	02/12 1200	02/13 0000	−3	0	+5	0	Y	N	2	180 S	540	590	13	2	−133	915	02/10 0230 H
02/14 0731	02/14 1200	02/16 0800	0	0	…	…	N	N	3	100 S	520	680	5	0	−67	815	02/12 0431 H
02/20 2139	02/21 0500	02/22 1200	0	0	+5	0	Y	…	2	120 S	380	460	15	2	−26	560	02/17 2006 H
03/01 0130	03/01 0300	03/02 0300	0	0	…	…	Y	…	1	20	480	530	8	0	−43	…	
03/18 2200	03/19 0200	03/19 1200	ns	ns	…	…	Y	Y	2	20	380	390	9	0	−3	…	
03/29 1100	03/29 1900	04/01 0000	0	+15	…	…	N	Y	2	280	420	590	7	0	−60	…	
04/06 1639	04/07 0600	04/08 0600	−7	−15	…	…	Y	…	2	220 S	560	620	6	1	−288	860	04/04 1632 H
04/18 2000	04/18 2000	04/19 1400	+8	0	…	…	N	…	3	30	460	470	10	1	−14	510	04/15 1035?
04/24 0400	04/24 0400	04/24 1300	0	0	…	…	N	…	3W	60	500	520	13	0	−61	…	
05/02 1045(A)	05/02 2000	05/05 1000	nc	ns	…	…	Y	…	3	150 S	500	860	6	0	−37	530	04/29 0430?
05/07 0000	05/07 0000	05/08 0000	+8	0	…	…	Y	Y	3W	10	400	420	8	0	−10	…	
05/13 1700	05/13 1700	05/14 1800	0	ns	…	…	N	…	2	100	500	600	8	0	−2	603	05/10 2006
05/15 1900	05/15 1900	05/16 1400	−2	0	…	…	N	…	3	20	430	450	8	0	−32	…	
05/16 2300	05/16 2300	05/17 0700	0	0	…	…	N	…	2	130	550	580	9	1	−92	500	05/13 1226
05/22 1700	05/23 0900	05/23 2100	0	nc	…	…	Y	Y	2	70	570	610	8	0	−10	830	05/20 1450
05/23 2342(W)	05/24 1200	05/27 1000	nc	0	…	…	Y	N	2	50 S	530	690	5	1	−147	650	05/21 0726
06/04 1502	06/04 2200	06/06 2200	−8	+6	…	…	Y	Y	3	130 S	470	560	9	0	−35	403	05/31 0806
06/08 0910	06/08 1200	06/10 1700	+24	+7	…	…	Y	Y	2	260 S	610	770	11	0	−90	1007	06/06 1554 H
06/11 0801	06/11 0900	06/11 1800	0	+6	…	…	Y	…	2	40 S	510	530	11	1	−36	…	
06/12 2208	06/13 1200	06/14 0600	nc	ns	…	…	N	N	2	60	440	550	4	0	−37	…	
06/18 0900	06/18 0900	06/18 1700	−3	+5	…	…	N	Y	3W	10	380	400	5	1	−12	…	
06/23 1303	06/24 0000	06/26 0800	0	nc	+3	−12	Y	Y	1	120 S	500	590	10	2	−34	…	
06/26 0000	06/26 1000	06/27 0000	0	+6	…	…	Y	Y	2	60	520	560	10	0	−76	…	

Major changes from Cane and Richardson (2003): D_{st} updated to final for all events; 01/18 Removed; 02/11 2352 Changed to magnetic cloud; 02/14 ICME leading edge and transit speed revised; 03/09 Removed; 04/06 ICME trailing edge revised; 04/18 Added; 04/27 Removed; 05/06 Disturbance changed to 05/07 0000; 05/23 Disturbance changed to 05/22 1700 and transit speed revised; 06/30 Removed.

Table 5 Near-Earth ICMEs in 2000, July–December.

Column 1 Disturbance mon/day UT	2 ICME Start mon/day UT	3 ICME End mon/day UT	4 Start C	5 End C	6 Start MC	7 End MC	8 BDE	9 BIF	10 Qual.	11 ΔV (km s^{-1})	12 V_I (km s^{-1})	13 V_{max} (km s^{-1})	14 B (nT)	15 MC?	16 D_{st} (nT)	17 V_{tr} (km s^{-1})	18 LASCO CME mon/day UT
2000																	
07/01 0100	07/01 0900	07/03 1700	+9	+4	0	−38	N	N	2	20	390	440	7	2	−11	…	
07/10 0638	07/11 0200	07/11 1400	0	+6	…	…	Y	Y	2	90 S	440	490	13	0	0	609	07/07 1026 H
07/11 1123(A)	07/11 2200	07/13 0300	0	0	0	0	Y	Y	1	30 S	520	540	10	2H	−26	…	
07/13 0942	07/13 1300	07/14 1500	…	…	0	−15	Y	N	3	200 S	610	670	7	2H	−43	940	07/11 1327 H
07/14 1532	07/14 1700	07/15 1400	0	0	+14	0	Y	N	2	150 S	780	800	9	2	−57	965	07/12 2030?
07/15 1437	07/15 1900	07/17 0800	0	+28	+2	−22	Y	N	2	350 S	740	1040	20	2	−301	1500	07/14 1054 H
07/19 1527	07/20 0100	07/21 0800	0	…	…	…	Y	N	2	100 S	530	630	8	0	−93	…	07/17 0854?
07/23 1041	07/23 1500	07/26 0500	0	0	…	…	N	N	3	20	360	430	9	0	−68	dg	dg
07/26 1857	07/27 0200	07/28 0200	0	−4	…	…	Y	Y	2	50 S	360	400	6	1	−42	490	07/23 0530
07/28 0634	07/28 1200	07/30 1300	+2	+30	+9	−27	Y	…	2	70 S	440	480	9	2	−71	550	07/25 0330 H
08/10 0501	08/10 1900	08/11 2100	0	nc	0	−13	Y	…	1	50 S	430	480	12	2H	−106	510	08/06 1830?
08/11 1845	08/12 0500	08/13 2200	−3	0	0	−17	Y	Y	1	120 S	580	670	18	2	−235	830	08/09 1630 H
09/02 2200	09/02 2200	09/03 1300	0	0	…	…	N	…	1	40	420	450	8	0	−20	418	08/29 1830?
09/08 1200	09/08 1200	09/10 1000	0	−18	…	…	Y	N	3	50	450	500	5	0	−48	530	09/05 0554
09/17 1657(A)	09/17 2100	09/21 0000	0	+12	+5	−54	Y	N	2	250 S	600	840	10	2	−201	…	09/15/16
10/03 0054	10/03 1000	10/05 0300	0	+3	+7	−13	Y	Y	1	60 S	400	430	14	2	−143	…	
10/05 0326	10/05 1300	10/07 1100	0	ns	…	…	Y	…	2	110 S	450	530	6	1	−182	756	10/02 2026 H
10/12 2228	10/13 1600	10/14 1700	−4	+3	+2	0	Y	…	1	120 S	400	460	12	2	−107	590	10/09 2350 H
10/28 0954	10/28 2100	10/29 2200	−9	+12	0	0	Y	Y	1	50 S	380	420	14	2	−127	565	10/25 0826 H
11/06 0948	11/06 1700	11/08 0300	0	0	+5	−9	Y	…	2	110 S	510	610	20	2	−159	660	11/3 1826 H
11/08 1200	11/08 1300	11/09 1500	0	0	…	…	Y	…	2	50	440	500	7	1	−36	…	
11/11 0400(A)	11/11 0800	11/12 0000	0	−14	…	…	N	Y	2	110 S	790	910	7	0	−37	1200	(11/09 1615)
11/26 1158	11/27 0800	11/28 0300	0	+8	…	…	Y	…	2	150 S	560	630	10	0	−80	…	11/24
11/28 0530	11/28 1100	11/29 2200	+11	0	…	…	Y	N	2	50 S	540	580	9	1	−119	720	11/25/26
12/21 1200	12/22 0300	12/22 2000	0	+4	…	…	Y	…	3W	40	290	330	4	0	−1	…	
12/22 1925	12/23 0000	12/23 1200	ns	ns	…	…	Y	…	3	50	320	330	12	0	−62	380	12/18 1150 H

Major changes from Cane and Richardson (2003): D_{st} updated to final for all events; 07/01 ICME times revised; 07/11 Changed to magnetic cloud (Huttunen *et al.*, 2005); 07/13 Changed to magnetic cloud (Huttunen *et al.*, 2005); 07/23 ICME trailing edge revised; 08/10 Changed to magnetic cloud (Huttunen *et al.*, 2005); 09/02 Disturbance changed to 2200; 09/08 ICME leading edge revised; 10/12 ICME leading edge revised; 10/20 Removed; 11/08 Added; 11/10 Removed; 12/21 Added; 12/22 Added.

Table 6 Near-Earth ICMEs in 2001, January–June.

Column 1 Disturbance mon/day UT	2 ICME Start mon/day UT	3 ICME End mon/day UT	4 Start C	5 End C	6 Start MC	7 End MC	8 BDE	9 BIF	10 Qual.	11 ΔV (km s^{-1})	12 V_I (km s^{-1})	13 V_{max} (km s^{-1})	14 B (nT)	15 MC?	16 D_{st} (nT)	17 V_{tr} (km s^{-1})	18 LASCO CME mon/day UT
2001																	
01/23 1048	01/24 0900	01/26 0700	0	ns	…	…	Y	…	2	140 S	400	550	4	1	−61	680	01/20 2130 H
03/03 1121	03/04 0400	03/05 0200	+12	0	+12	0	N	…	2	50 S	440	520	8	2H	−73	610	02/28 1450
03/19 1114	03/19 1700	03/22 0000	0	+12	+6	+15(2)	Y	Y	1	100 S	360	490	15	2	−149	520	03/16 0350
03/27 0110(A)	03/27 2000	03/28 1700	0	0	0	−12	Y	…	2	80 S	610	650	12	2H	−87	…	
03/27 1747	03/28 1700	03/30 1800	+11	0	…	…	Y	Y	3	200 S	480	560	3	0	−51	850	03/25 1706 H
03/31 0052	03/31 0500	03/31 2200	0	nc	…	…	Y	N	3	200 S	640	710	33	1	−387	690	03/28 1250 H
03/31 2200	04/01 0400	04/03 1500	nc	0	…	…	Y	Y	2	200	600	820	5	1	…	700	03/29 1026 H
04/04 1455	04/04 1800	04/05 1200	0	+6	0	−4	Y	N	2	90 S	650	780	9	2	−50	1020	04/02 2206
04/08 1101	04/08 1400	04/09 0400	0	0	…	…	Y	…	3	100 S	740	780	13	0	−59	1050	04/06 1930 H
04/11 1343	04/11 2200	04/13 0700	0	0	+10	−13	Y	Y	2	230 S	640	740	14	2	−271	1290	04/10 0530 H
04/13 0734	04/13 0900	04/14 1200	0	−6	…	…	Y	Y	1	200 S	730	830	9	0	−77	990	04/11 1331 H
04/15 1700	04/15 1700	04/16 0100	ns	ns	…	…	SEP	N	2W	0	500	510	4	0	−36	…	
04/18 0046	04/18 1200	04/20 1100	ns	ns	…	…	Y	…	2	140 S	430	520	8	0	−114	…	
04/21 1601	04/21 2300	04/23 0300	ns	ns	0	−2	N	N	1	50 S	350	390	11	2	−102	…	
04/28 0501	04/28 1400	05/01 0200	0	+32	+12	−37	N	Y	2	400 S	550	730	8	2	−47	1040	04/26 1230 H
05/03 1100	05/03 1100	05/04 1000	0	0	…	…	Y	…	2W	0	380	390	8	0	−2	…	
05/07 0800	05/07 1900	05/08 0700	0	+12	…	…	Y	Y	2	30	360	410	8	1	−25	…	
05/08 1101	05/09 1200	05/10 2200	0	nc	…	…	N	N	2	50 S	430	560	8	1	−76	…	
05/11 1300	05/11 1300	05/12 0000	…	…	…	…	N	N	2W	0	430	430	8	0	−48	…	
05/27 1459	05/28 0300	05/31 1400	+8	0	+9	−52	N	N	2	100 S	420	590	7	2	−42	…	
06/07 0852(A)	06/07 1800	06/08 0700	ns	ns	…	…	N	N	1	50 S	390	430	9	1	−8	…	
06/27 0300	06/27 0300	06/28 1700	0	ns	…	…	N	…	1	20	420	490	3	1	−18	…	

Major changes from Cane and Richardson (2003): D_{st} updated to final for all events; 03/03 Changed to magnetic cloud (Huttunen *et al.*, 2005); 03/27 0110 Added, magnetic cloud (Huttunen *et al.*, 2005); 03/27 1747 ICME leading edge revised; 03/31 2200 ICME trailing edge revised; 04/04 ICME leading and trailing edges revised; 04/08 ICME leading and trailing edges revised; 04/15 Added; 04/18 Transit speed removed; 05/03 Added; 05/12 Removed; 05/15 Removed; 05/27 ICME trailing edge revised; 05/30 Merged with 05/27; 06/21 Removed; 06/26 Disturbance time changed to 06/27 0300.

Table 7 Near-Earth ICMEs in 2001, July–December.

Column 1 Disturbance mon/day UT	2 ICME Start mon/day UT	3 ICME End mon/day UT	4 Start C	5 End C	6 Start MC	7 End MC	8 BDE	9 BIF	10 Qual.	11 ΔV (km s^{-1})	12 V_I (km s^{-1})	13 V_{max} (km s^{-1})	14 B (nT)	15 MC?	16 D_{st} (nT)	17 V_{tr} (km s^{-1})	18 LASCO CME mon/day UT
2001																	
07/08 1200	07/09 0200	07/11 0400	0	−12	+39	+29	Y	…	2	30	400	460	5	2	−38	520	07/05 0354
07/13 1700	07/13 1700	07/14 0100	0	0	…	…	N	…	2	20	400	420	8	1	−4	…	
08/03 0716	08/03 1100	08/03 1400	0	+20	…	…	Y	…	3	60 S	420	440	10	0	−13	…	
08/15 0500	08/15 0500	08/16 1400	ns	ns	…	…	N	…	3W	0	390	450	5	0	−16	…	
08/17 1103	08/17 2000	08/19 1600	0	0	…	…	Y	…	2	150 S	500	600	11	0	−105	620	08/14 1601 H
08/30 1411	08/30 1700	08/31 1000	0	0	…	…	Y	…	3W	50 S	420	500	6	1	−40	…	
09/01 1300	09/01 1300	09/02 2200	0	0	…	…	N	…	2	0	360	410	5	1	−17	…	
09/13 0231(W)	09/13 1800	09/14 2200	0	4	…	…	Y	…	2	30 S	410	440	10	1	−57	…	
09/23 2000	09/24 0000	09/24 2200	+8	−4	…	…	N	…	3W	30	440	530	7	1	−73	570	09/20 1931
09/25 0000	09/25 0600	09/25 2000	0	0	…	…	SEP	…	2	30	380	400	5	0	−24	…	
09/29 0940	09/29 1100	10/01 0000	+10	0	…	…	Y	…	2	180 S	560	700	12	1	−66	790	09/27 0454?
09/30 1924	10/01 0800	10/02 0000	ns	ns	…	…	Y	…	2	80 S	490	550	9	0	−148	710	09/28 0854 H
10/01 2200	10/02 0400	10/02 1200	0	0	…	…	Y	…	2	40	490	520	8	0	−104	715	09/29 1154
10/02 1200	10/02 1400	10/03 1600	0	+8	+11	0	Y	…	2	30	500	530	12	2H	−166	…	
10/04 1400	10/04 1400	10/05 1900	nc	nc	…	…	N	…	3	0	420	470	3	0	…	…	
10/11 1701	10/12 0400	10/12 0900	−7	0	…	…	Y	…	2	180 S	560	570	22	1	−71	780	10/09 1130 H
10/21 1648	10/21 2000	10/25 1000	0	0	…	…	Y	…	1	250 S	460	680	9	0	−187	870	10/19 1650 H
10/26 2200	10/27 0300	10/28 1200	0	nc	…	…	Y	…	3	20	420	500	10	0	−27	417	10/22 1826
10/28 0319	10/29 2200	10/31 1300	−6	+7	…	…	N	…	2	150 S	360	510	5	0	−157	694	10/25 1526
10/31 1348	10/31 2000	11/02 1200	ns	ns	0	−2	Y	…	2	60 S	330	390	11	2	−106	…	
11/05 1000	11/05 1900	11/6 0600	0	0	…	…	SEP	…	2	30	420	430	18	1	−73	…	
11/06 0152	11/06 1200	11/09 0300	0	−39	…	…	Y	…	2	300 S	600	750	7	1	−292	1250	11/04 1635 H
11/19 1815	11/19 2200	11/21 1300	0	0	…	…	Y	…	3W	130 S	430	570	6	1	−47	680	11/17 0530 H
11/24 0656	11/24 1400	11/25 2000	0	−6	0	−6	Y	…	2	550 S	720	1040	14	2	−221	1320	11/22 2330 H
12/28 0000	12/28 0000	12/29 1200	+5	−6	…	…	Y	…	2	10	360	370	8	0	−10	…	
12/29 0538	12/30 0000	12/30 1800	−14	−6	…	…	N	…	3	90 S	400	460	16	1	−58	580	12/26 0530?

Major changes from Cane and Richardson (2003): D_{st} updated to final for all events; 08/27 Removed; 09/23 Disturbance changed to 2000; 09/25 Added; 09/29 ICME leading edge revised; 10/01 ICME leading and trailing edges revised; 10/02 Added; 10/04 Added; 10/26 ICME leading and trailing edges revised; 11/05 Added; 11/06 ICME leading and trailing edges revised; 11/24 ICME trailing edge revised; 11/27 Removed.

Table 8 Near-Earth ICMEs in 2002.

Column 1 Disturbance mon/day UT	2 ICME Start mon/day UT	3 ICME End mon/day UT	4 Start C	5 End C	6 Start MC	7 End MC	8 BDE	9 BIF	10 Qual.	11 ΔV (km s^{-1})	12 V_I (km s^{-1})	13 V_{max} (km s^{-1})	14 B (nT)	15 MC?	16 D_{st} (nT)	17 V_{tr} (km s^{-1})	18 LASCO CME mon/day UT
2002																	
02/28 0451	02/28 1700	03/02 0000	0	+16	0	−14	Y	N	2	80 S	390	410	11	2H	−71	…	
03/18 1322	03/19 0500	03/20 1600	0	0	+18	0	Y	N	2	160 S	380	470	15	2	−37	667	03/15 2306
03/20 1328	03/21 1400	03/22 0600	0	−8	…	…	Y	…	3	210 S	440	580	8	0	−13	…	
03/23 1137	03/24 1200	03/25 2000	0	+4	0	+2	Y	…	2	70 S	450	500	15	2	−100	625	03/20 1706?
04/12 0100	04/12 0100	04/13 1300	0	0	…	…	N	N	3W	0	420	450	8	1	−32	…	
04/17 1107	04/17 1600	04/19 1500	0	0	+11	−13	Y	…	1	150 S	480	610	14	2	−127	750	04/15 0350
04/19 0835	04/20 0000	04/21 1800	0	−6	+12	0	Y	…	1	200 S	500	640	8	2	−149	863	04/17 0826 H
05/11 1014	05/11 1500	05/12 0000	0	0	…	…	N	…	2	90 S	430	440	15	1	−110	610	05/08 1350 H
05/20 0340	05/20 1000	05/21 2200	−7	−8	…	…	Y	Y	3	70 S	420	510	7	1	−36	420	05/16 0050 H
05/23 1050	05/23 2000	05/25 1800	…	…	+3	−25	Y	…	2	400 S	590	920	11	2	−109	1323	05/22 0326 H
07/17 1603	07/18 1200	07/19 0900	0	nc	…	…	Y	N	3	100 S	460	520	6	1	−17	955	07/15 2030 H
07/19 1450(A)	07/20 0200	07/22 0600	0	0	…	…	Y	…	2	650 S	650	930	7	0	−36	…	
07/31 1100	07/31 2200	08/01 0900	0	nc	…	…	Y	…	3	40	410	460	10	0	−21	…	
08/01 0510	08/01 0900	08/01 2300	+2	+5	+3	0	N	…	2	70 S	450	460	12	2	−51	…	
08/01 2309	08/02 0600	08/04 0200	0	0	+3	−29	Y	…	2	60 S	460	520	10	2	−102	500	07/29 1207
08/18 1846	08/19 1200	08/21 1400	−7	+38	…	…	Y	…	2	160 S	460	580	8	1	−106	766	08/16 1230 H
08/29 2100	08/29 2100	08/30 0600	+6	nc	…	…	N	…	2W	0	400	420	8	1	−42	…	
09/07 1200	09/07 1200	09/08 0400	0	0	…	…	Y	N	2	0	380	400	8	1	−41	…	
09/07 1636	09/08 0400	09/08 2000	nc	0	…	…	Y	…	2	170 S	470	550	11	0	−181	880	09/05 1654 H
09/08 2000	09/08 2200	09/10 2100	+18	+15	…	…	N	…	2	50	440	520	9	1	−82	…	
09/19 0600	09/19 2000	09/20 2100	0	ns	…	…	Y	Y	2	80	520	750	5	0	−40	910	09/17 0806
09/30 0815	09/30 2000	10/01 1500	0	+12	+2	−2	Y	…	2	70 S	390	410	23	2	−176	…	
10/02 2210(A)	10/03 0100	10/04 1800	0	+6	…	…	N	…	2	80 S	430	520	11	1	−146	…	
11/16 2305(A)	11/17 1000	11/19 1200	0	nc	…	…	Y	…	2	20 S	380	500	10	1	−52	…	
12/17 1800	12/17 1800	12/19 1200	0	0	…	…	Y	N	2	0	380	430	14	0	−30	…	
12/20 1700	12/21 0300	12/22 1900	0	0	…	…	N	Y	2	30	440	540	11	0	−75	…	

Major changes from Cane and Richardson (2003): D_{st} updated to final for all events; 02/15 Removed; 02/28 Changed to magnetic cloud (Huttunen *et al.*, 2005); 03/23 ICME leading edge revised; 04/17 ICME leading and trailing edges revised; 05/11 Added; 05/20 ICME leading edge revised; 05/21 Removed; 07/31 Added; 09/07 1200 Added; 09/30 Added; 11/16 ICME trailing edge revised; 12/17 Added; 12/20 Added.

Table 9 Near-Earth ICMEs in 2003.

Column 1 Disturbance mon/day UT	2 ICME Start mon/day UT	3 ICME End mon/day UT	4 Start C	5 End C	6 Start MC	7 End MC	8 BDE	9 BIF	10 Qual.	11 ΔV (km s^{-1})	12 V_I (km s^{-1})	13 V_{max} (km s^{-1})	14 B (nT)	15 MC?	16 D_{st} (nT)	17 V_{tr} (km s^{-1})	18 LASCO CME mon/day UT
2003																	
01/26 0000	01/27 0100	01/28 1400	−4	+7	0	−23	Y	…	2	60	500	720	9	2H	−20	…	
02/01 1305(A)	02/01 1900	02/03 0700	…	0	…	…	Y	…	2	340 S	510	760	11	0	−72	820	01/30 1006
02/17 2150(A)	02/18 0400	02/19 1600	0	0	…	…	Y	…	1	70 S	600	700	8	0	−17	…	
03/20 0440	03/20 1200	03/20 2200	0	0	0	0	Y	…	1	100 S	650	810	11	2	−64	…	
05/09 0455(A)	05/09 0700	05/11 0000	0	+12	…	…	N	…	2	100 S	680	900	8	1	−84	…	
05/29 1224	05/29 1300	05/29 1800	0	nc	…	…	Y	…	3	70 S	650	680	10	1	−49	…	
05/29 1825(A)	05/30 0200	05/30 1600	nc	0	…	…	Y	…	3	120 S	600	760	20	1	−144	999	05/28 0050 H
05/30 1600(A)	05/30 2200	06/01 0100	−3	−19	…	…	Y	…	3	220 S	680	780	7	0	−63	1078	05/29 0127 H
06/15 1500	06/15 2000	06/16 2100	+6	0	…	…	Y	…	3	80	510	590	10	1	−68	dg	dg
06/16 1800	06/17 1000	06/18 0800	0	0	+8	0	N	…	3	80	480	540	10	2	−141	650	06/14 0154
07/23 1400	07/23 1400	07/24 1600	0	0	…	…	N	…	2	90	430	500	6	1	−26	…	
08/04 1700	08/04 2200	08/06 0200	+5	0	…	…	Y	…	2	0	440	500	9	1	−60	…	
08/15 1200	08/16 0200	08/17 1600	−9	0	…	…	N	…	2	70	490	620	7	1	−11	…	
08/17 1421	08/18 0100	08/19 1500	0	+18	+10	−10	Y	…	1	80 S	450	530	18	2	−148	630	08/14 2006 H?
10/21 2200	10/22 0200	10/24 1500	0	nc	…	…	Y	…	2	100	520	740	9	1	−61	…	
10/24 1524	10/24 2100	10/25 1200	nc	nc	…	…	Y	Y	2	140 S	560	600	21	1	−36	760	10/22 0830
10/25 1100	10/25 1400	10/26 0400	nc	…	…	…	Y	…	3	40	490	610	13	0	−49	…	
10/26 1908	10/26 2200	10/28 0000	0	0	…	…	Y	…	2	90 S	470	540	10	1	−52	…	
10/28 0206	10/28 0230	10/28 0900	ns	ns	…	…	Y	N	1	130 S	610	620	19	0	−32	1331	10/26 1754
10/29 0611	10/29 1100	10/30 0300	0	nc	0	0	Y	Y	2	900 S	1300	1900	32	2H	−353	2185	10/28 1130 H
10/30 1619(A)	10/31 0200	11/02 0000	0	+24	…	…	Y	…	2	750 S	800	1700	9	1	−383	2138	10/29 2054 H
11/20 0803	11/20 1000	11/21 0800	0	+8	0	−6	Y	N	2	240 S	580	700	28	2	−422	886	11/18 0850 H

Table 10 Near-Earth ICMEs in 2004.

Column 1 Disturbance mon/day UT	2 ICME Start mon/day UT	3 ICME End mon/day UT	4 Start C	5 End C	6 Start MC	7 End MC	8 BDE	9 BIF	10 Qual.	11 ΔV ($\mathrm{km\,s^{-1}}$)	12 V_{I} ($\mathrm{km\,s^{-1}}$)	13 $V_{\max}$ ($\mathrm{km\,s^{-1}}$)	14 B (nT)	15 MC?	16 D_{st} (nT)	17 V_{tr} ($\mathrm{km\,s^{-1}}$)	18 LASCO CME mon/day UT
2004																	
01/09 1500	01/10 0600	01/11 0500	−12	0	…	…	N	N	2	60	560	620	10	1	−60 P	…	
01/22 0137	01/22 0800	01/23 1700	0	−5	…	…	Y	Y	2	200 S	560	680	12	0	−149 P	850	01/20 0006 H
01/23 1425(A)	01/23 2300	01/25 0400	0	+2	…	…	Y	Y	2	60 S	490	550	10	1	−89 P	720	01/21 0454 H
02/17 1800	02/17 1800	02/18 1600	…	0	…	…	N	N	2	0	440	460	8	0	−26 P	…	
04/03 0900(A)	04/03 1400	04/05 1800	0	0	+12	−3	Y	N	1	40 S	440	520	15	2	−112 P	560	dg(03/31 1036)
04/26 1604	04/26 1700	04/27 2000	…	…	…	…	N	…	2	50	460	500	6	1	−6 P	dg	dg
04/30 1300	05/01 0000	05/01 1200	ns	ns	…	…	N	…	2	40	430	450	9	0	−36 P	dg	dg
05/01 1200	05/01 1500	05/02 2100	0	0	…	…	Y	…	2	30	400	430	9	1	−15 P	dg	dg
07/22 1036	07/22 1800	07/24 0800	0	…	−3	−35	Y	…	2	90 S	560	670	11	2	−101 P	920	07/20 1331 H
07/24 0613	07/24 1400	07/25 1500	…	nc	0	0	Y	N	2	90 S	560	610	20	2	−148 P	890	07/22 0731
07/25 1500	07/25 2000	07/26 2200	nc	…	…	…	Y	Y	2	110	640	680	6	1	…	890	07/23 1606 H
07/26 2249	07/27 0200	07/27 2200	0	+10	0	−10	Y	…	1	300 S	870	1000	16	2	−197 P	1302	07/25 1454 H
08/01 0100	08/01 0900	08/02 0400	0	0	…	…	N	…	3	40	440	520	6	1	−42 P	…	
08/29 0909(W)	08/29 1900	08/30 2200	ns	+10	0	0	N	…	1	40 S	390	440	12	2	−126 P	…	
09/13 2003	09/14 1500	09/16 1200	−6	0	…	…	Y	…	3W	110 S	550	600	6	1	−50 P	960	09/12 0036 H
09/17 2100	09/18 1200	09/20 0000	0	0	…	…	N	Y	3	20	400	440	6	1	−43 P	500	09/14 1010 H
11/07 1827	11/07 2200	11/09 1000	0	nc	+4	−17	Y	Y	1	140 S	630	720	18	2	−373 P	720	11/04 2330
11/09 1825(W)	11/09 2000	11/11 2300	0	0	0	−36(2)	SEP	…	1	170 S	640	810	14	2	−289 P	830	11/07 1654 H
11/11 1710	11/12 0800	11/13 2300	0	0	…	…	Y	…	2	60	520	670	7	1	−109 P	1080	11/10 0226 H
12/11 1340	12/12 2200	12/13 1900	0	0	…	…	Y	…	2	60	400	580	13	0	−61 P	640	12/8 2026 H
12/27 0500	12/27 1600	12/29 0200	+24	0	…	…	Y	N	3	80	440	560	7	1	−48 P	dg	dg

Table 11 Near-Earth ICMEs in 2004.

Column 1 Disturbance mon/day UT	2 ICME Start mon/day UT	3 ICME End mon/day UT	4 Start C	5 End C	6 Start MC	7 End MC	8 BDE	9 BIF	10 Qual.	11 ΔV (km s^{-1})	12 V_I (km s^{-1})	13 V_{max} (km s^{-1})	14 B (nT)	15 MC?	16 D_{st} (nT)	17 V_{tr} (km s^{-1})	18 LASCO CME mon/day UT
2005																	
01/07 0922	01/07 1500	01/08 1200	0	0	…	…	N	N	2	60	520	570	17	1	−96 P	550	(01/04 0616)
01/08 1700	01/08 2100	01/09 1800	0	−10	…	…	N	Y	2	40	460	520	9	1	…	570	01/05 1530 H
01/16 1100	01/16 1400	01/17 0700	0	0	…	…	Y	N	3	80	520	580	8	1	−70 P	640	01/13 1754 H
01/18 2100	01/18 2300	01/20 0300	−2	+10	…	…	Y	Y	1	…	800	960	12	0	−93 P	1170	01/17 0930 H
01/21 1711	01/21 1900	01/22 1700	0	−5	…	…	Y	N	2	340 S	810	960	19	0	−105 P	1210	01/20 0654 H
01/31 0900	01/31 1400	02/02 0900	ns	ns	…	…	N	N	2	120	560	660	8	0	−36 P	…	
02/17 2200	02/18 1400	02/19 0600	0	0	…	…	Y	…	1	50	530	580	6	0	−86 P	…	
02/20 1200	02/20 1200	02/22 0700	ns	ns	…	…	N	…	3	0	410	440	5	1	−48 P	500	02/17 0006 H
02/22 1000	02/22 1400	02/23 1900	ns	0	…	…	N	N	3	30	380	400	9	0	−12 P	…	
05/15 0238	05/15 0600	05/19 0000	0	0	0	−74	Y	N	2	400 S	630	950	15	2	−263 P	1270	05/13 1712 H
05/20 0300	05/20 0300	05/22 0200	0	+20	+4	−21	N	…	2	30	430	480	10	2	−103 P	488	05/16 1350
05/28 0436	05/29 0300	05/29 1500	+3	nc	…	…	N	…	2	60 S	400	490	11	1	−44 P	…	
05/29 0952	05/30 0100	05/30 2300	nc	nc	…	…	N	…	2	130 S	460	540	15	1	−138 P	630	05/26 1506 H
05/30 2300	05/31 0400	06/01 0300	nc	0	…	…	N	…	3	30	460	490	4	0	…	430	05/26 2126
06/12 0745	06/12 1500	06/13 1300	0	0	0	−6	N	…	2	80	480	510	14	2	−106 P	650	06/09 1436
06/14 1835	06/15 0500	06/16 0900	nc	0	0	0	Y	N	2	100 S	480	560	9	2	−54 P	…	
06/16 0847	06/16 1700	06/17 1900	0	0	…	…	Y	Y	3	230 S	600	680	7	1	−48 P		
07/10 0337	07/10 1000	07/12 0400	0	+28	…	…	Y	…	2	80 S	430	480	12	1	−94 P	720	07/07 1706
07/17 0134	07/17 1400	07/18 2300	ns	ns	0	−19	N	…	2	50 S	420	500	8	2	−76 P	…	
08/09 0000	08/09 0000	08/09 1900	0	0	…	…	Y	…	2	40	480	520	6	1	−18 P	477	08/05 0854
08/10 0600	08/10 0600	08/10 1100	0	0	…	…	N	…	2	20	440	460	8	1	−53 P	…	

Table 11 (*Continued*)

Column 1	2	3	4	5	6	7	8	9	10	11	12	13	14	15	16	17	18
Disturbance mon/day UT	ICME Start mon/day UT	ICME End mon/day UT	Start C	End C	Start MC	End MC	BDE	BIF	Qual.	ΔV (km s^{-1})	V_I (km s^{-1})	V_{max} (km s^{-1})	B (nT)	MC?	D_{st} (nT)	V_{tr} (km s^{-1})	LASCO CME mon/day UT
08/23 2000	08/24 0000	08/24 1100	0	0	…	…	N	N	3	30	440	460	20	1	−5 P	…	
08/24 0613	08/24 1400	08/24 2300	0	0	…	…	Y	N	2	100 S	660	710	20	1	−216	790	08/22 0131H
09/02 1419	09/02 1800	09/03 0400	0	nc	…	…	Y	Y	2	110 S	650	680	10	1	−48 P	840	08/31 1130
09/11 0114	09/11 0500	09/12 0700	0	nc	…	…	Y	…	2	300 S	900	1100	10	0	−147 P	1423	09/9 1948
09/12 0605(A)	09/12 2000	09/13 1300	−6	0	…	…	Y	…	2	230 S	750	980	7	0	−90 P	…	
09/13 0900	09/13 1600	09/14 0800	0	ns	…	…	Y	…	3	60	630	740	5	0	−95 P	…	
09/15 0600	09/15 0600	09/16 1800	0	0	…	…	Y	…	3	0	680	860	7	1	−86 P	…	
09/20 1800	09/20 1800	09/21 1800	…	ns	…	…	N	N	2W	0	350	390	6	0	−34 P	…	
10/31 0200	10/31 0200	10/31 1900	ns	ns	0	0	N	…	2	20	360	400	11	2	−75 P	…	
12/31 0000	12/31 0400	01/01 1700	0	+4	+9	−6	Y	…	2	30	480	550	8	2	−45 P	…	

Table 12 Near-Earth ICMEs in 2006–2009.

Column 1	2	3	4	5	6	7	8	9	10	11	12	13	14	15	16	17	18
Disturbance mon/day UT	ICME Start mon/day UT	ICME End mon/day UT	Start C	End C	Start MC	End MC	BDE	BIF	Qual.	ΔV ($\mathrm{km\,s^{-1}}$)	V_{I} ($\mathrm{km\,s^{-1}}$)	$V_{\max}$ ($\mathrm{km\,s^{-1}}$)	B (nT)	MC?	D_{st} (nT)	V_{tr} ($\mathrm{km\,s^{-1}}$)	LASCO CME mon/day UT
2006																	
02/05 2000	02/05 2000	02/06 1200	ns	+3	0	0	N	…	2	30	340	360	10	2	−22 P	…	
04/13 1100	04/13 1500	04/14 0700	0	0	0	+2(2)	Y	…	2	120	520	550	18	2	−111 P	540	04/10 0606?
04/14 1300	04/14 1300	04/14 2100	0	0	…	…	N	…	2	20	500	540	9	0	…	…	
07/09 2136	07/10 2100	07/11 1900	0	0	…	…	N	…	1	100 S	380	430	8	0	−23 P	488	07/06 0854 H
08/19 1131	08/20 1300	08/21 1600	−7	+14	…	…	N	…	2	90 S	400	470	8	0	−71 P	620	08/16 1630 H
08/30 2000	08/30 2000	09/01 0700	…	ns	0	−16	Y	…	3	0	400	540	8	2	−34 P	440	08/26 2057
09/30 0300	09/30 0800	09/30 2000	ns	ns	0	0	N	…	3	90	400	440	15	2	−18 P	…	
11/01 1700	11/01 1700	11/02 1400	ns	ns	…	…	Y	…	3W	0	380	410	5	0	−19 P	…	
11/18 1000	11/18 1000	11/20 0200	…	…	…	…	N	…	3W	30	400	430	9	0	−13 P	…	
11/28 1300	11/29 0500	11/30 1000	0	0	…	…	N	…	3	20	420	500	12	2	−74 P	…	
12/14 1414	12/14 2200	12/15 1300	0	+7	0	+7	Y	…	1	320 S	740	900	13	2	−146 P	1180	12/13 0254 H
12/15 2000	12/15 2000	12/16 1900	0	…	…	…	N	…	2	90	620	650	3	0	…	…	
12/16 1755	12/17 0000	12/17 1700	…	+24	…	…	N	…	3	70 S	580	680	4	0	−37 P	980	12/14 2230 H
2007																	
01/14 1248	01/14 1200	01/15 0700	ns	ns	…	…	N	…	1	60	360	380	12	2	−51 Q	…	
11/19 1811	11/19 2300	11/20 1200	−4	0	0	0	Y	…	1	30	460	480	18	2	−63 Q	437	11/15 1806 H?
2008																	
09/17 0000	09/17 0400	09/18 0800	0	0	…	…	Y	…	2	10	400	490	6	1	−22 Q	…	09/12 (S)
12/04 0400	12/04 1200	12/05 1100	…	…	…	…	N	…	3	40	390	510	7	1	−39 Q	…	
12/16 1159	12/17 0300	12/17 1400	ns	ns	…	…	N	…	3	30	350	380	9	1	−26 Q	350	12/12 0435 (S)

Table 12 (*Continued*)

Column 1 Disturbance mon/day UT	2 ICME Start mon/day UT	3 ICME End mon/day UT	4 Start C	5 End C	6 Start MC	7 End MC	8 BDE	9 BIF	10 Qual.	11 ΔV ($km\,s^{-1}$)	12 V_I ($km\,s^{-1}$)	13 V_{max} ($km\,s^{-1}$)	14 B (nT)	15 MC?	16 D_{st} (nT)	17 V_{tr} ($km\,s^{-1}$)	18 LASCO CME mon/day UT
2009																	
01/18 2100	01/19 0200	01/19 0500	0	0	…	…	N	…	2	40	430	450	12	1	−3 Q	…	
01/25 2224	01/26 1000	01/26 1500	…	…	…	…	Y?	…	3W	50	340	380	10	1	−32 Q	320	01/20 1200? (S)
06/03 1600	06/04 0200	06/05 1600	ns	ns	…	…	…	…	3W	20	310	330	5	1	−20 Q	…	
06/27 1400	06/27 1600	06/28 1600	ns	ns	…	…	…	…	2	30	390	420	7	1	−25 Q	380	06/23 01 (S)
07/20 1400	07/21 0100	07/22 0200	…	…	…	…	…	…	2	20	330	350	8	1	−79 Q	…	
09/30 0100	09/30 0600	10/01 0000	…	…	…	…	…	…	3	50	340	360	7	1	−5 Q	…	
10/29 0500	10/29 0500	10/29 2300	…	…	…	…	…	…	3	20	370	390	11	1	−2 Q	…	
11/13 2000	11/14 1000	11/15 0000	…	…	…	…	…	…	2	20	310	330	7	1	−19 Q	410	11/9 $\approx$ 14? (S)
12/12 0500	12/12 2000	12/13 2200	…	…	…	…	…	…	2	30	270	300	6	1	−5 Q	…	
12/19 1000	12/19 1300	12/20 1700	…	…	…	…	…	…	3W	20	380	430	4	0	−5 Q	…	

Column 8 indicates whether or not bidirectional suprathermal electrons were observed within the ICME (Y/N = yes/no), based on our assessment of the SWEPAM electron pitch-angle plots from the ACE Science Center. For events before the launch of ACE, and events where SWEPAM observations are dominated by solar energetic particles, we examined 260 eV electron pitch-angle plots from the WIND 3DP instrument (http://sprg.ssl.berkeley.edu/wind3dp/). In a few cases, indicated by "SEP", we could not assess the presence of BDEs in either data set because of the presence of solar energetic particles. Overall, 67% of the ICMEs (205/308) where we can assess the data show evidence of BDEs.

Column 9 indicates the presence of bidirectional energetic ion flows (BIFs) observed by the IMP 8 GME (for the ICME commencing on 31 October 2003, the BIFs are reported by Malandraki *et al.* (2005)). Here, "..." indicates that either there are no data for a given ICME, the available data cover a limited region of the ICME such that it is not possible to assess whether any bidirectional flows were present, particle counts are insufficient to be able to assess the particle flows, or IMP 8 was inside the bow shock. "Y" or "N" indicate that there is, or is no, evidence (in the available data, which may not extend throughout the ICME interval) of bidirectional flows. Overall, energetic ion flows can be examined for 114 ICMEs, of which 66 (58%) show evidence of BIFs.

The remaining columns are largely similar to those in Cane and Richardson (2003). Column 10 indicates the overall "quality" of the ICME boundary time estimates, where '1' is the most reliable. In some cases this has changed from Cane and Richardson (2003). For example, consideration of the SWICS data may help to clarify the ICME boundaries. A "W" indicates a marginal event with weak ICME signatures. Column 11 (not included in Cane and Richardson (2003)) shows the increase in solar wind speed at the upstream disturbance (to the nearest 10 km s^{-1}) estimated from 1-hour averaged data. An 'S' indicates that a shock reported in the ACE or Kasper shock lists contributed to this speed increase (which may be larger than the actual speed increase at the shock if for example, the solar wind speed increased further following the shock). Of the 322 ICMEs, 163 (51%) have identified upstream shocks. Note that in a few cases (*e.g.*, 4 May 1998), there is a large increase in solar wind speed but no shock is reported. Typically, the speed transition is too gradual to be associated with a true shock.

Columns 12 to 14 give the average ICME speed based on the plasma/field ICME intervals, the maximum post-shock solar wind speed (*i.e.*, between the shock/disturbance and plasma/field ICME trailing edge), and the average magnetic field strength within the plasma/field ICME, to the nearest 1 nT.

A '2' in Column 15 indicates that the ICME includes a magnetic cloud reported on the WIND magnetic cloud list or by Huttunen *et al.* (2005) ("2H"). In a few cases, an indicated magnetic cloud is not reported on these lists, but the magnetic field characteristics of the ICME are, in our assessment, consistent with those for a magnetic cloud (*e.g.*, enhanced intensity >10 nT, smooth rotation through a large angle, low proton temperatures, Klein and Burlaga, 1982). A '1' indicates that there is evidence of a rotation in the magnetic field direction, but overall, the magnetic field characteristics do not meet those of a magnetic cloud. Events with no magnetic cloud-like magnetic field features are indicated by '0'.

The minimum geomagnetic D_{st} value is given in Column 16. Here, 'P' indicates that the value is provisional, and 'Q' that the value is obtained from the "Real-time (Quick-look)" D_{st} index provided by the World Data Center for Geomagnetism, Kyoto University (http://swdcwww.kugi.kyoto-u.ac.jp/). Otherwise, final values are given. The period considered for each event extends from the disturbance to the trailing edge of the ICME signatures or slightly beyond if a storm driven by the trailing regions of an ICME reaches peak intensity just after ICME passage. Here "..." indicates that strong geomagnetic activity is already in progress and there is no further intensification associated with the ICME. See Zhang *et al.* (2007), Echer *et al.* (2008), Zhang, Poomvises, and Richardson (2008), Zhang, Richardson, and Webb (2008), and Richardson and Zhang (2008) for further discussion of the relationship between ICMEs and intense ($D_{\mathrm{st}} \leq -100$ nT) storms during most of cycle 23.

The shock transit speed to 1 AU is given in Column 17 if we can identify the probably-associated solar event, indicated in Column 18. The event time generally corresponds to first observation of the related CME by the LASCO coronagraphs on the SOHO spacecraft, where ‘H’ denotes that this is reported as a halo CME in the online CME catalogue (http://cdaw.gsfc.nasa.gov/CME_list/). A gap in LASCO observations that encompasses the likely time of the associated solar event is indicated by “dg”. SOHO EIT movies and other data (*e.g.*, Hα flares) are used to help infer the solar source regions of the CMEs. Times in brackets are for the associated solar flares if there are no LASCO observations. A range of dates indicates that there are several CMEs in a reasonable time window at the Sun and it is difficult to identify the specific CME responsible for the ICME. In some cases, there are multiple CMEs, but the time of the most likely association is given. Solar sources for the subset of events associated with intense geomagnetic storms are discussed by Zhang *et al.* (2007), while Cane, Erickson, and Prestage (2002), Cane *et al.* (2006) and Cane, Richardson, and von Rosenvinge (2010) have summarized the sources of large solar energetic particle events in 1997 – 2006, some of which are related to ICMEs at Earth. A few recent associations, indicated by ‘S’, are based on observations of Earthward-directed CMEs made by the SECCHI coronagraphs on the STEREO spacecraft (http://secchi.nrl.navy.mil/).

One caveat is that we may not have been able to delineate every *individual* ICME that is present. Two circumstances can present particular difficulties. The first is at times of high solar activity, when multiple ICMEs and shocks pass by the Earth and the interplanetary observations are especially complicated. Even after consideration of the various data sets, it may not be possible to identify every individual structure. Thus, some ICME regions listed may include multiple ICMEs. The second is when an extended ICME region has a complicated structure, such as the “complex ejecta” discussed by Burlaga *et al.* (2001) and Burlaga, Plunkett, and St. Cyr (2002). Again, it may not be clear how many ICMEs may contribute. As Burlaga, Plunkett, and St. Cyr (2002) note, although multiple CMEs at the Sun may contribute in producing these extended ICMEs, it may be difficult to identify features in the ICME that correspond to individual component CMEs. In some cases, LASCO halo CME observations can help to indicate how many ICMEs might be expected to be observed subsequently at Earth. However, since it is clear from comparing observations of halo CMEs and near-Earth ICMEs that some reported halo CMEs do not encounter the Earth, other ICMEs have no halo CME counterpart, some halo CMEs in the LASCO catalog originate from activity far from central meridian and are unlikely to be Earthward-directed, and others occur on the far side of the Sun, we are cautious in using halo CME reports as a guide to interpreting the numbers of ICMEs subsequently present at Earth. Further examination of the coronagraph images is required to assess how many of these CMEs are likely to be Earthward-directed. In summary, we are generally cautious about interpreting the origin of substructures that might be present within the ICMEs listed in the catalog.

The footnotes to Tables 1 to 12 indicate the major changes from the Cane and Richardson (2003) catalog, including events removed or added and significant (several-hour) changes in the disturbance or ICME times. Minor changes in these times or other parameters are not noted. Comparing the Cane and Richardson (2003) catalog for 1996 – 2002 and the current revised catalog, the largest annual difference in the number of events is 5, in 1999 (*cf.* 33 events in this year in Table 3). Hence overall, revision of the catalog taking into account additional data sets has had little impact on the number of identified ICMEs (see also Figure 5 of Richardson and Cane (2005b)).

Figure 5 Solar source longitudes for ICMEs in this study (positive = west of central meridian), based predominantly on Hα observations.

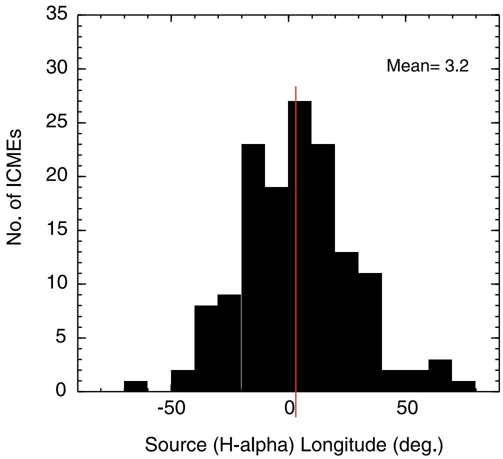

4. Properties of ICMEs during Cycle 23

4.1. Solar Source Longitudes

As is evident in Tables 1 to 12 and as previously noted by Cane, Richardson, and St. Cyr (2000) and Cane and Richardson (2003), the associated solar events cannot be identified for nearly a half (46%) of the ICMEs at Earth, based on observations of halo or partial halo CMEs by LASCO, or Hα and X-ray flare reports. Figure 5 shows the solar source longitude distribution with respect to central meridian for those ICMEs for which the source can be identified. As found in previous studies (see, *e.g.*, Richardson and Cane, 1993; Cane, Richardson, and St. Cyr, 2000; Cane and Richardson, 2003), the sources of near-Earth ICMEs are predominantly close to central meridian. Around 95% lie within 50° of central meridian and 64% within 20°. There is a slight excess of western sources, with 43% lying on the eastern hemisphere, and 57% on the western; the mean location is W3.2 ± 2.0°. There are also six sources beyond W50° compared with only one beyond E50°. This asymmetry is consistent with the systematic eastward deflection of ICMEs expected when they interact with the Parker spiral interplanetary magnetic field (see, *e.g.*, Gosling *et al.*, 1987b), but might also, for example, be due to other factors, such as a possible tendency for CMEs to be released to the east of the associated Hα flares (Wang *et al.*, 2002). Overall, the results suggest that ICMEs may extend in longitude up to ≈50° from the solar source.

4.2. ICME Rate

Panel (a) of Figure 6 summarizes the ICME rate/solar (Carrington) rotation, for individual rotations and averaged over three running rotations, during 1996 – 2009. The monthly mean sunspot number (SSN) is plotted in panel (b). As previously noted by Cane and Richardson (2003), the *yearly* ICME rate increased by over an order of magnitude from solar minimum to solar maximum, from 4 year^{-1} in 1996 to a peak of 51 year^{-1} in 2000. However, the ICME rate/Carrington rotation in Figure 6 may be characterized as increasing to ≈2 – 3/rotation in 1996 – 1997, then remaining at a similar level during much of the period from 1998 to late 2005, approximately corresponding to SSN > 40. In addition, there are occasional intervals of enhanced ICME rates associated with periods of exceptionally high solar activity (such as July 2000, early-2001). Figure 6 also suggests that the ICME rate increased again in

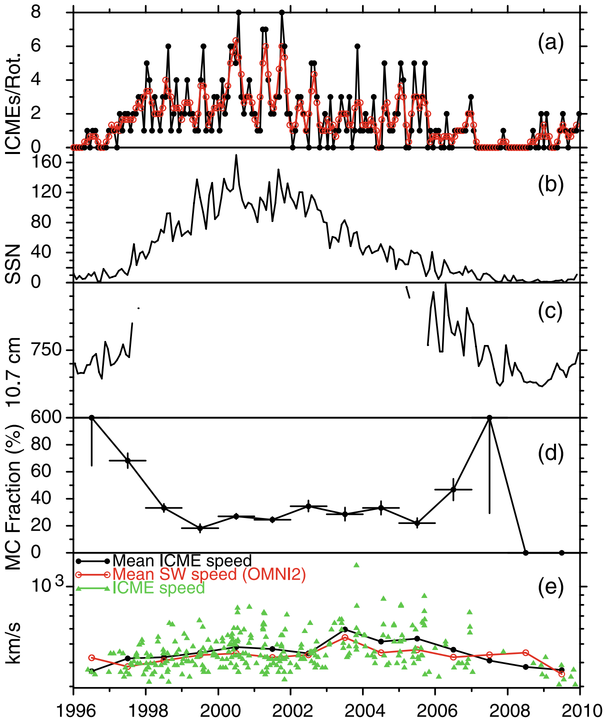

Figure 6 Panel (a) shows the ICME rate (/solar rotation) and 3-rotation running mean (red) for 1996 to 2009. Below are: (b) the monthly sunspot number, (c) Penticton solar 10.7 cm flux, (d) fraction of ICMEs that are magnetic clouds, and (e) the mean solar wind and ICME speeds in each year and the speeds of individual ICMEs.

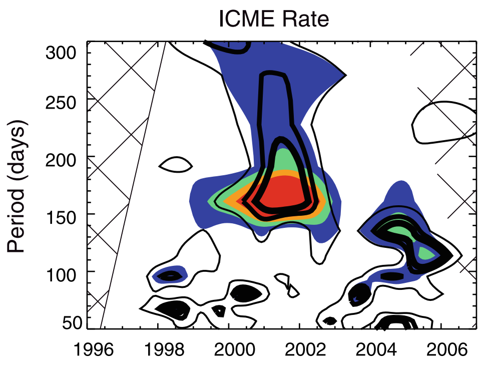

Figure 7 Wavelet analysis of the ICME rate power (color scale, red is highest) as a function of period and time during 1996 – 2007. Regions with significance levels of 70%, 90% and 95% are indicated by increasingly thicker overlaid contours.

mid-2008 after around a year and a half with few identified ICMEs during the unusually extended solar minimum at the end of cycle 23. Although SSN remained close to zero, the solar 10.7 cm radio flux illustrated in panel (c) (the range is intentionally limited to low flux levels) shows a small upturn in 2009 suggesting that this increased ICME activity is a harbinger of solar cycle 24.

Figure 7 shows an update of the results of Richardson and Cane (2005a) using wavelet analysis (Torrence and Compo, 1998) to examine "quasi-periodic" features in the ICME rate and their variation with time during 1996 – 2007 (there are insufficient events to extend the analysis to later years). The power level, shown for periods of 50 – 300 days, is indicated by the color scale (red is highest, white lowest) which is arbitrary and linear. Edge effects may be present in the "cone of influence" indicated by the hatched areas. Regions with significance levels of 70%, 90% and 95% are indicated by increasingly thicker overlaid contours (see Richardson and Cane (2005a) for further details of the application of wavelet analysis to these data). The greatest power in the ICME rate occurred in an "island" of enhanced power centered at ≈160 days and extending from ≈140 to 180 days, during ≈1999 to 2002, as previously noted by Richardson and Cane (2005a). The new feature in Figure 7 is the region of enhanced power at ≈110 – 150 days in late 2003 – 2006, suggesting the presence of quasi-periodicities in the ICME rate during the declining phase of the cycle. Rieger *et al.* (1984) first identified quasi-periodicities of ≈150 days in gamma-ray and X-ray flares in solar cycle 21, and similar quasi-periodicities (with periods of ≈130 – 185 days, Lean, 1990) have now been recognized in a number of solar and interplanetary phenomena during several solar cycles (see, *e.g.*, Richardson and Cane (2005a) for further details). The features in Figure 7 appear to be consistent with this type of quasi-periodicity. The origin of the quasi-periodicity is uncertain, one possibility being that it is related to Rossby-type waves in the Sun (see, *e.g.*, Lou, 2000; Dimitropoulou, Moussas, and Strintzi, 2008; Zaqarashvili *et al.*, 2010).

4.3. Fraction of Magnetic Clouds

Based on observations during this and the previous two solar cycles, we have previously noted (Cane and Richardson, 2003; Richardson and Cane, 2004b) evidence of a solar-cycle dependence in the fraction of ICMEs that have the characteristics of magnetic clouds, with the fewer ICMEs around solar minimum having a higher incidence of MCs than ICMEs around solar maximum. Panel (d) of Figure 6 shows the magnetic cloud fraction for the events in Tables 1 to 12. The decline in the magnetic cloud fraction from the start of the cycle previously reported is again evident. However, the situation is less clear during the extended minimum at the end of cycle 23, at least up to the end of the period shown, with few ICMEs meeting the criteria to be magnetic clouds.

One difference from the results in Cane and Richardson (2003) and Richardson and Cane (2004b) is that the number of ICMEs identified as magnetic clouds is increased due to additional events added to the WIND magnetic cloud list since the times of these studies, and the events discussed by Huttunen *et al.* (2005). Thus, the magnetic cloud fraction during much of the cycle except around solar minimum is now closer to the often quoted 30% based on the results of Gosling (1990).

Figure 8 shows the magnetic cloud fraction calculated for events in 10° bins in solar source longitude out to 40° from central meridian, and for events at 40 – 90°. The "error bars" indicate the effect of changing the number of magnetic clouds and ICMEs by ± one event. Although the statistics are poor in some longitude ranges, there is a suggestion of an increase in the magnetic cloud fraction, from ≈30% to ≈50%, for events originating within ≈20° west of central meridian. This result may be consistent with a scenario in which a magnetic cloud forms the central "core" of an ICME, together with the systematic eastward deflection of ICMEs in the solar wind discussed above. In this case, we might expect the core of the ICME to be observed more frequently for events originating on the western solar hemisphere.

4.4. Comparison of CME and 1 AU Disturbance Transit Speeds

For each of the solar event-ICME pairs, the inferred 1 AU transit speed *of the disturbance* is shown in Tables 1 to 12. The corresponding 1 AU transit time is shown in Figure 9 plotted vs. the (plane of the sky) expansion speed of the related CME observed by LASCO. As has

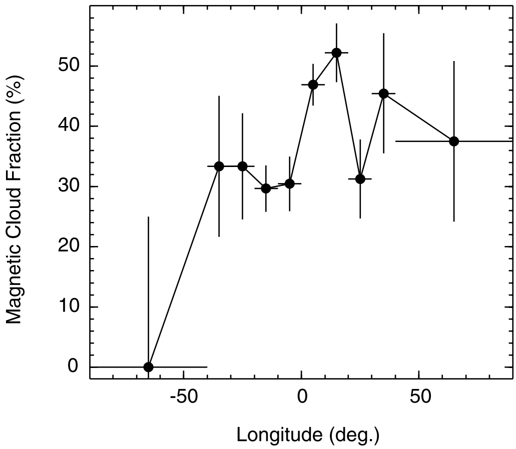

Figure 8 Magnetic cloud fraction plotted against solar source longitude.

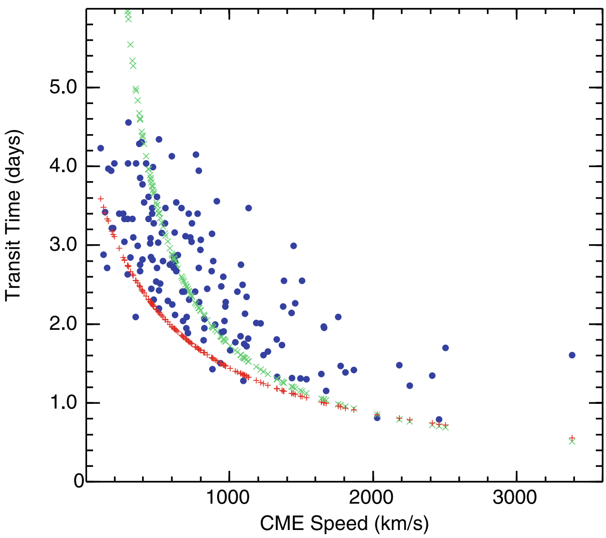

Figure 9 Disturbance 1 AU transit time plotted against the CME plane of the sky expansion speed observed by LASCO. The green plus signs indicate the transit time for each event assuming travel at the CME expansion speed, while the red crosses assume a transit speed $V_{\text{tr}} = 400 + 0.8 V_{\text{CME}}$ (Cane and Richardson, 2003), which gives a good estimate of the earliest disturbance arrival time for a given CME speed.

been shown previously for subsets of ICMEs in cycle 23 (see, *e.g.*, Cane, Richardson, and St. Cyr, 2000; Gopalswamy *et al.* 2000, 2001; Michalek *et al.*, 2004; Schwenn *et al.*, 2005), there is a general anti-correlation between the 1 AU transit time (either of the disturbance, used here, or of the ICME leading edge, used in some of these other studies) and the CME expansion speed, but with much scatter. Furthermore, this trend is inconsistent with the assumption that the ICME moves away from the Sun with a constant speed equal to that of the CME (the green points in Figure 9 indicate the transit times for the events with this assumption). Rather, the observations are more consistent with a deceleration of fast CMEs and an acceleration of slow CMEs, converging on the solar wind speed.

There have been considerable efforts to understand the various factors that may contribute to the event-to-event scatter in the transit times and obtain an empirical formula to "predict" the mean arrival time of CME-related disturbances and/or ICMEs at Earth (see, *e.g.*, Gopalswamy *et al.*, 2000; Vršnak and Gopalswamy, 2002; Michalek *et al.*, 2004; Schwenn *et al.*, 2005). From the point of view of space weather forecasting, it may be interesting (and simpler) to infer the earliest time at which an ICME, or more specifically, the related disturbance since this is the first interplanetary effect associated with the ICME, might reach the Earth following a CME with a certain (plane of the sky) speed (which will not necessarily correspond to the speed in the Earthward direction). In Cane and Richardson (2003), we suggested that the fastest disturbance transit speed for a given CME speed may be given by $V_{\mathrm{tr}}(\mathrm{km\,s^{-1}}) = 400 + 0.8V_{\mathrm{CME}}$, based on the events included in that study. In Figure 9, we plot the transit time implied by this relationship as red crosses, and note that it gives a reasonable estimate of the earliest disturbance arrival time for this extended set of ICMEs. We therefore suggest that this relationship could be used to "forecast" the earliest time that the influence of a CME could be experienced in the near-Earth solar wind.

The event shown with the highest CME speed (on 11 November 2004, associated with a 3387 km s^{-1} CME at 0226 UT on 10 November according to the LASCO CME catalog) has a transit time that is around a day longer than the shortest transit time that would be expected for this CME speed. However, the CACTUS catalog (http://sidc.oma.be/cactus/) suggests a less extreme CME speed, with a maximum speed of 1994 km s^{-1} based on LASCO observations. The LASCO "observers log" also reports a similar speed. Assuming a "true" CME speed of ≈2000 km s^{-1} would still imply a transit time that is longer than the minimum expected, but one that is also consistent with other events with similar CME speeds.

4.5. *In-situ* Speed

Panel (e) of Figure 6 shows the average *in-situ* speed for each ICME together with the average speed for all ICMEs in a given year (black graph). Average ICME speeds increased by around 100 km s^{-1}, from ≈400 to 500 km s^{-1}, in 1996 – 2003, then declined again in 2006 – 2007. At least two factors may contribute to this solar cycle variation. One is the variation in average solar wind speeds also shown in this panel (red graph, from the OMNI data set), since ICME speeds tend to converge towards the ambient solar wind speed. Another factor is the tendency for fast ICMEs to occur more frequently following solar maximum in this cycle, as is evident from inspection of Figure 6 (see also Cane *et al.*, 2006). Note also that during the extended solar minimum, no ICMEs with speeds significantly exceeding average solar wind speeds were observed from December 2006 until at least the end of 2009.

Distributions of the ICME speed and other parameters are shown in Figure 10. ICME speeds (panel (a)) range from ≈290 to 1300 km s^{-1}, with a mean of 476 ± 6 km s^{-1} (the error is in the mean of all events). This value is comparable to mean speeds at 1 AU of 458 km s^{-1} and 456 km s^{-1} implied by the studies of the variation in ICME properties with heliocentric distance by Liu, Richardson, and Belcher (2005) and Wang, Du, and Richardson (2005), and with the mean of 483 km s^{-1} at 1 AU we obtained in a study of ICMEs at 0.3 – 1 AU observed in 1975 – 1980 that is summarized in Section 3 of Forsyth *et al.* (2006). These results are summarized in Table 13 together with those for other ICME parameters. (See also Gopalswamy (2006) for discussion of the parameters of subsets of the ICMEs in cycle 23.)

4.6. Magnetic Field Intensity

The magnetic field intensity distribution is in Figure 10, panel (b). Considering all the ICMEs, the mean field is 10.1 ± 0.3 nT, compared with 12.6 ± 0.4 nT in magnetic clouds (see also Wu and Lepping, 2007) and 8.9 ± 0.3 nT in non-cloud ICMEs. For comparison, the all solar wind average for the study period is 6.35 ± 0.01 nT. The 1 AU mean ICME field intensities implied by the results of Liu, Richardson, and Belcher (2005) and Wang,

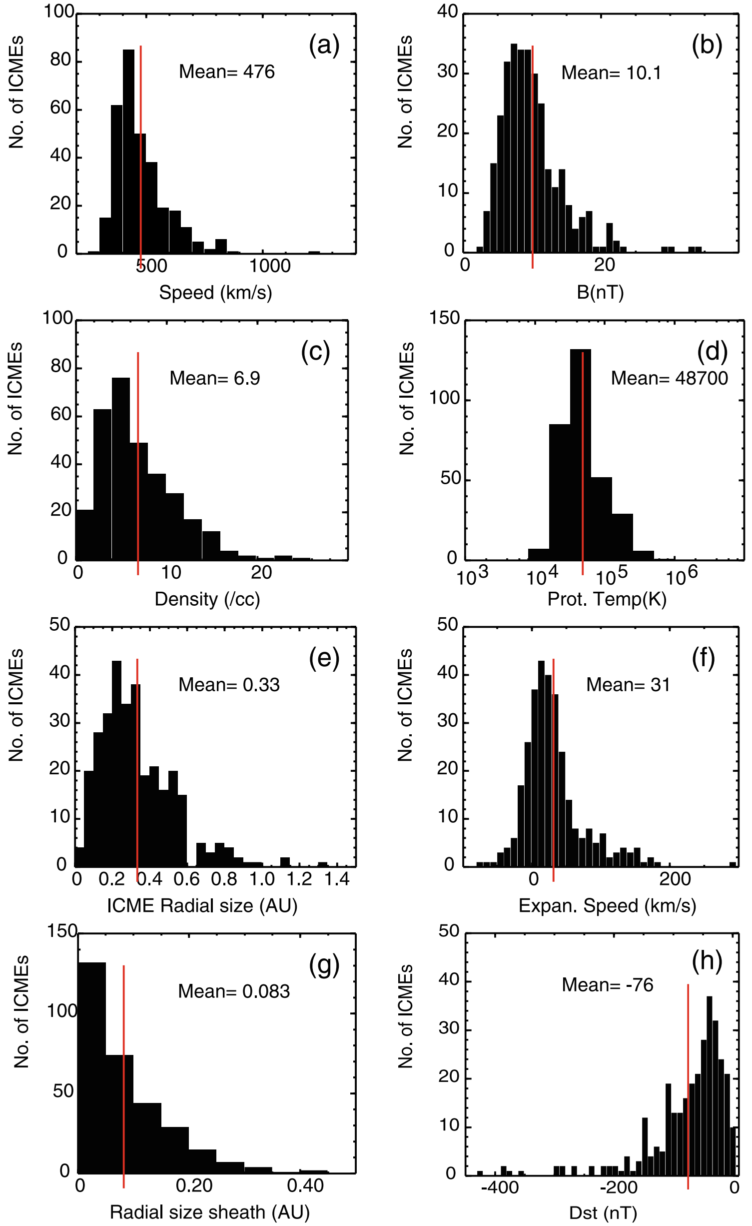

Figure 10 Distributions of mean ICME parameters and minimum value of the D_{st} index.

Du, and Richardson (2005), who make no distinction between magnetic clouds and non-cloud ICMEs, are $\approx$2 nT below our average values, while our result reported in Forsyth *et al.* (2006) (10.3 nT) based on a sample of ICMEs from cycle 21 is remarkably similar to that of the current study. Combining all these results, a reasonable summary is that magnetic clouds have average field strengths around twice average solar wind values, while non-cloud ICMEs have more modest enhancements, of the order of 30%. Table 13 also includes the

Table 13 Average 1 AU ICME parameters.

	BS98[a]	F06[b]	L05[c]	W05[d]	L07[e]	This work
S(AU)	0.24	0.31	0.25	0.19	0.195 ± 0.017[f]	0.33 ± 0.01
n (cm^{-3})	6.47	7.03	6.16	6.7	6.63 ± 0.28	6.9 ± 0.2
V (km s^{-1})		483	458	456		476 ± 6
T (10^3K)		44.3	35.4	29.2	28.5 ± 3.2	48.7 ± 2.9
Mean B (nT)		10.3	7.35	8.3	18.1 ± 1.4[g]	10.1 ± 0.3
V_{ex}		39.7	57.5	$0.12 V_{ICME}$		31 ± 3

[a]Bothmer and Schwenn (1998), magnetic clouds, 0.3 – 1.0 AU.

[b]Section 3 of Forsyth *et al.* (2006), 0.3 – 1.0 AU.

[c]Liu, Richardson, and Belcher (2005), 0.3 – 5.4 AU.

[d]Wang, Du, and Richardson (2005), 0.3 – 5.4 AU.

[e]Leitner *et al.* (2007), magnetic clouds, 0.3 – 6 AU.

[f]fitted magnetic cloud diameter.

[g]axial magnetic field.

mean *axial* field strength (18.1 ± 1.4 nT) for magnetic clouds at 1 AU inferred from the results of Leitner *et al.* (2007). This is ≈50% larger than the mean magnetic field strength we obtain along the spacecraft trajectory in ICMEs including a magnetic cloud, and reasonably consistent with the ≈35% difference found by Leitner *et al.* (2007).

There is a modest correlation (cc = 0.60) between the maximum magnetic field strength in those ICMEs that include magnetic clouds and the ICME speed at 1 AU (Figure 11, left-hand panel). Note that fields >30 nT are found in magnetic clouds with speeds of ≈600 km s^{-1} or more. However, there are also fast magnetic clouds without strongly enhanced magnetic fields, at least along the spacecraft trajectory through the cloud. The correlation between speed and maximum field intensity is much weaker (cc = 0.28) for non-cloud ICMEs (Figure 11, right-hand panel). See also Owens *et al.* (2005) for discussion of the relationship between ICME magnetic field intensities and speeds.

4.7. Density

The average density for all the ICMEs is 6.9 ± 0.2 cm^{-3} (distribution is in Figure 10, panel (c)), consistent with the 1 AU densities from the studies summarized in Table 13. Previous work (see, *e.g.*, Richardson *et al.*, 2000) has shown that exceptionally low solar wind densities tend to be more frequently found within ICMEs. Using the 1-hour OMNI data, we find that in our study period, densities ≤1 cm^{-3} comprised 8.5% of measurements within magnetic clouds and 6.0% in non-cloud ICMEs, compared with only 0.9% of those in the ambient (non-ICME) solar wind, again indicating that low plasma densities are more likely to be encountered inside ICMEs. Overall, 43% of solar wind densities ≤1 cm^{-3} occurred within ICMEs.

4.8. Proton Temperature

The mean ICME-averaged proton temperature (distribution is in Figure 10, panel (d)) is $48\,700 \pm 2900$ K, compared with $76\,300 \pm 400$ K for the ambient solar wind in our study period. This result is comparable to the 44 300 K at 1 AU inferred from Helios ICMEs quoted

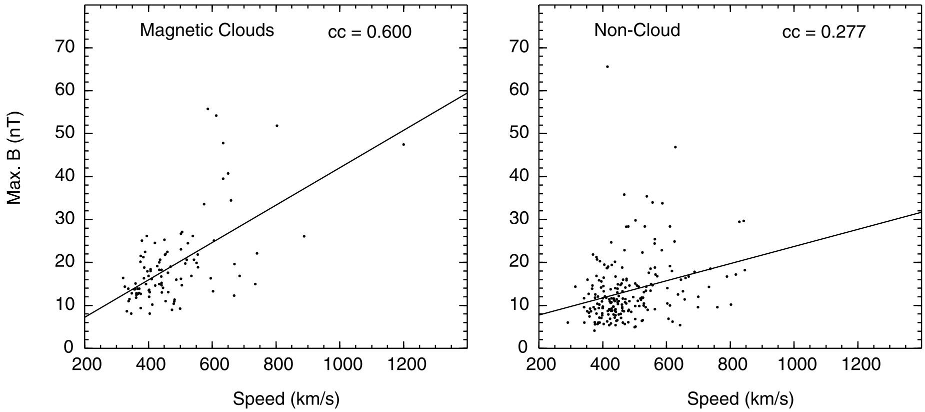

Figure 11 Maximum magnetic field strength plotted against speed at 1 AU for ICMEs that include (left) or do not include (right) magnetic clouds.

in Section 3 of Forsyth *et al.* (2006) but higher than the 1 AU values implied by the results of Liu, Richardson, and Belcher (2005) and Wang, Du, and Richardson (2005). A possible explanation is that the latter studies used low proton temperatures as a primary parameter for ICME identification whereas we have considered a range of parameters and hence may identify occasional ICMEs in which the proton temperature is not strongly depressed but there are other ICME signatures (for example, enhanced O^7/O^6 in the case of the 8 April 2001 ICME). Similarly, the lower mean temperature reported by Leitner *et al.* (2007) may arise because their study only included magnetic clouds, and a depressed proton temperature is one criterion for a magnetic cloud.

4.9. ICME and Sheath Radial Size, and ICME Expansion Speed

The mean ICME radial size along the line of the spacecraft trajectory relative to the ICME, obtained by integrating the solar wind speed with time during ICME passage (as defined by the plasma/field signatures, columns 3 and 4 of Tables 1 to 12) is 0.33 ± 0.01 AU (distribution is in Figure 10, panel (e)). This is reasonably comparable to the mean sizes obtained by the other studies summarized in Table 13. Remarkably, 59 events (19%) have radial sizes exceeding 0.5 AU, and three events (4 May 1998, 17 September 2000, and 15 May 2005) exceed 1.0 AU. The unusual durations of the 4 May 1998 and 17 September 2000 events have also been noted by Burlaga *et al.* (2001) and Burlaga, Plunkett, and St. Cyr (2002), respectively. Burlaga, Plunkett, and St. Cyr (2002) suggest that the latter event may have resulted from the coalescence of four CMEs though they note that these CMEs appear to have "merged and lost their separate identity", although one clearly had a flux rope structure. The 4 May 1998 event was also preceded by multiple CMEs that might have contributed to the extended ICME, in addition to the most prominent CME given in Table 2. Again, it is difficult to identify substructures within the ICME. The solar phenomena associated with the 15 May 2005 ICME, have been described by Yurchyshyn *et al.* (2006) and Liu *et al.* (2007) who suggest that this was an isolated solar event during a relatively quiet period. However, Dasso *et al.* (2009) proposed that two solar events were involved, resulting in two magnetic clouds followed by an extended region of ICME-like plasma. We note that composition/charge state data, not considered by Dasso *et al.* (2009), suggest that ICME-like plasma extended for another $\approx$1.5 days beyond the region that they identified.

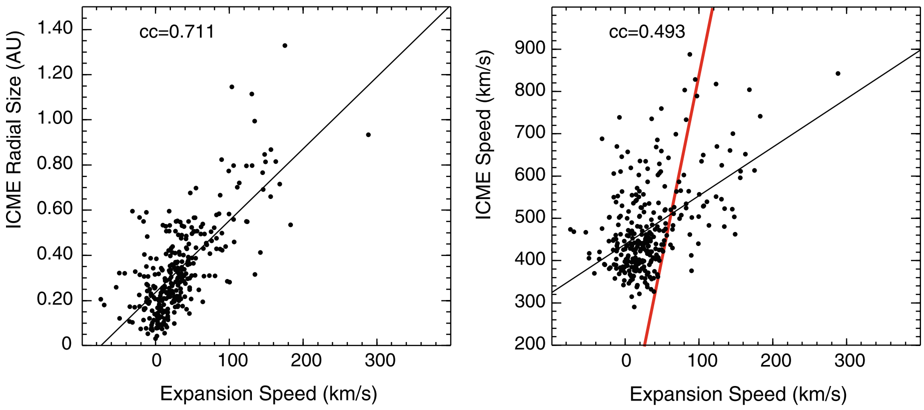

Figure 12 ICME radial size or speed plotted against expansion speed. The red line indicates the $V_{ex} = 0.12 V_{ICME}$ dependence found by Wang *et al.* (2005).

Returning to Table 13, the mean magnetic cloud diameter obtained from model flux rope fits to the field data by Leitner *et al.* (2007) is only around 55% of our average ICME radial size. This difference may be consistent with the observations in Figure 2 and columns 6 and 7 of Tables 1 – 12 that show that some magnetic clouds may be only substructures of larger ICME-like intervals.

Panel (f) of Figure 10 shows the distribution of the ICME expansion speed, defined as half of the difference in solar wind speeds at the beginning and end of the ICME interval. The predominance of positive values indicates that most ICMEs are expanding at 1 AU. The mean expansion speed is $31 \pm 3\ \mathrm{km\,s^{-1}}$, or $43 \pm 3\ \mathrm{km\,s^{-1}}$ if only positive values are considered, reasonably consistent with the $39.7\ \mathrm{km\,s^{-1}}$ and $57.5\ \mathrm{km\,s^{-1}}$ mean expansion speeds reported in Forsyth *et al.* (2006) and Liu, Richardson, and Belcher (2005), respectively for other groups of ICMEs. The left-hand panel of Figure 12 shows a good correlation (cc = 0.71) between the ICME radial size and ICME expansion speed. The expansion speed is more weakly correlated (cc = 0.49) with the mean ICME solar wind speed (Figure 12, right-hand panel), and does not appear to be consistent with the $V_{ex} = 0.12 V_{ICME}$ dependence suggested by Wang, Du, and Richardson (2005) (red line). Considering the mean ICME magnetic field strength (10.0 nT) and density ($6.9\ \mathrm{cm^{-3}}$) gives an Alfvén speed of $76\ \mathrm{km\,s^{-1}}$. Thus, the mean expansion speed is around half the Alfvén speed based on average ICME parameters, consistent with the earlier conclusion of Klein and Burlaga (1982).

Démoulin *et al.* (2008), Démoulin (2010) and Gulisano *et al.* (2010) have discussed a self-similar expansion of ICMEs in terms of a dimensionless expansion factor $\zeta = (2V_{ex} D/\Delta t) V_c^{-2}$ (taking into account a factor of two difference in their definition of the expansion speed), where D is the heliocentric distance, Δt is the duration of the ICME and V_c is the speed at the center of the ICME. This expression is approximately $\zeta = 2V_{ex} D/(SV)$ where V is the average ICME speed and S is the radial size ($= V\Delta t$). Figure 13 shows the distribution of ζ for 243 of our ICMEs with positive expansion speeds. The distribution is broader and with a smaller average value (0.45) than that obtained by Démoulin (2010) (average 0.81 ± 0.19) for a sample of "unperturbed" magnetic clouds, suggesting that in general our ICMEs (which, however, are not restricted to magnetic clouds) do not expand following this prescription.

Considering the thickness of the sheath upstream of the ICME along the spacecraft trajectory, the distribution in panel (g) of Figure 10 shows that the occurrence rate falls of with

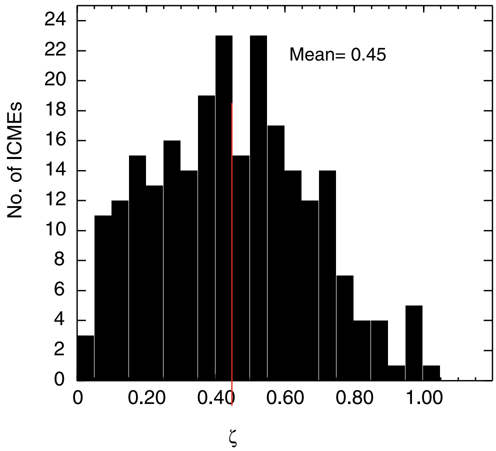

Figure 13 Distribution of the dimensionless expansion factor defined by Démoulin (2010) for the expanding ICMEs in this study.

increasing thickness. The mean is 0.082 ± 0.005 AU, *i.e.*, about one quarter of the average ICME size. Rarely, the sheath may extend up to $\approx$0.4 AU. Of course, this ICME study does not include cases where only the flank of an interplanetary shock and an extended sheath is encountered, but not the related ICME, a situation expected to be more frequently observed far from the solar event longitude (see, *e.g.*, Borrini *et al.*, 1982; Cane, 1988; Richardson and Cane, 1993).

4.10. Geomagnetic Activity

The intensity of geomagnetic activity associated with our ICMEs is indicated by the distribution of the minimum value of the geomagnetic D_{st} index shown in panel (h) of Figure 10. The average minimum D_{st} is -76 nT, while the most probable value is ≈ -40 nT. Exceptionally intense and exceptionally quiet activity levels are both relatively rare. Some 81 ICMEs (26%) are associated with "intense" storms with $D_{\mathrm{st}} \leq -100$ nT, and 18 (6%) have $D_{\mathrm{st}} \leq -200$ nT. We note though (see, *e.g.*, Zhang *et al.*, 2007) that these storms may involve not only the listed ICME but also the associated sheath, additional ICMEs, interactions with corotating high-speed streams, and shocks traveling though these structures.

Figure 14(a) shows the good anti-correlation (cc $= -0.891$) between the maximum value of the southward magnetic field component (B_{s}) in the sheath or ICME (based on 1-hour averaged data) and the intensity of the associated geomagnetic activity, as measured by the minimum value of the D_{st} index. The best fit is given by $D_{\mathrm{st}} = -8.23B_{\mathrm{s}} + 3.74$ (D_{st} and B_{s} are in nT). Figure 14(b) shows the much weaker correlation (cc $= -0.539$) between minimum D_{st} and V_{max} which is driven primarily by the few exceptionally fast events (similar results are obtained using ICME or 1 AU transit speeds). Figure 14(c) shows the high correlation (cc $= -0.903$) between minimum D_{st} and the maximum positive value of the y-component of the solar wind electric field ($E_y = -B_z V$, in GSM coordinates) in the sheath or ICME (from the 1-hour averaged OMNI data set). The best fit is given by $D_{\mathrm{st}}(\mathrm{nT}) = -11.9E_y(\mathrm{mV\,m^{-1}}) - 13.3$. Correlations between D_{st} and B_{s} or E_y have been noted previously for intense storms in cycle 23 (see, *e.g.*, Echer *et al.*, 2008) but here we demonstrate that these correlations also hold for ICMEs/sheaths that generate lower levels of geomagnetic activity. Figure 14(d) shows the probability that an ICMEs/sheath will give rise to an intense ($D_{\mathrm{st}} \leq -100$ nT) or $D_{\mathrm{st}} \leq -200$ nT storm as a function of maximum E_y. These results, which may be of interest for storm forecasting, suggest that there is a

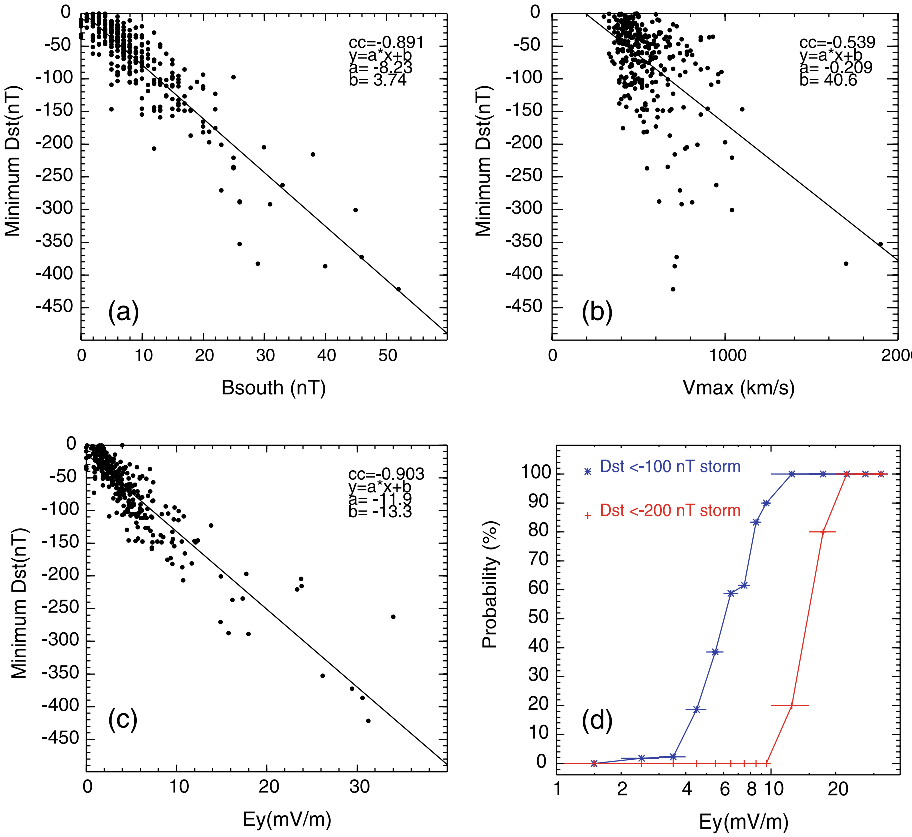

Figure 14 (a) Minimum D_{st} plotted against the magnitude of the maximum southward magnetic field component in the ICME or preceding sheath for 300 ICMEs (correlation coefficient = 0.891). (b) Minimum D_{st} plotted against the maximum speed in the ICME or upstream sheath (cc = 0.539). (c) Minimum D_{st} plotted against the maximum value of E_y in the sheath or ICME (cc = 0.903). (d) Probability of an ICME being associated with a $D_{\mathrm{st}} < -100$ nT or < -200 nT storm as a function of maximum E_y.

$>50\%$ probability of generating an intense storm if the maximum 1-hour averaged value of E_y in an ICME or the associated sheath exceeds ≈ 6 mV m^{-1}, and that all cases with $E_y > 10$ mV m^{-1} generate intense storms. The probability of generating a $D_{\mathrm{st}} < -200$ nT storm is $\approx 20\%$ for $E_y = 10-15$ mV m^{-1}, rising to $\approx 80\%$ for $E_y = 15-20$ mV m^{-1}.

Figure 15 shows minimum D_{st} plotted against the ICME solar source longitude. The ICMEs associated with 10 out of the 11 geomagnetic storms with minimum $D_{\mathrm{st}} < -250$ nT originated within 20° of central meridian, and those associated with $D_{\mathrm{st}} < -150$ nT storms, within 40° of central meridian. Hence, there is a strong preference for the ICMEs related with severe geomagnetic storms to originate close to central meridian (see also Figure 8 of Zhang *et al.* (2007)). Considering just the ICMEs originating within 20° of central meridian, 48% were associated with intense storms ($D_{\mathrm{st}} < -100$ nT). Although this result might suggest that around a half of ICMEs originating near central meridian are associated with such storms, it should be noted that only ICMEs for which the source location can be identified are considered here. There are presumably other events from central meridian among

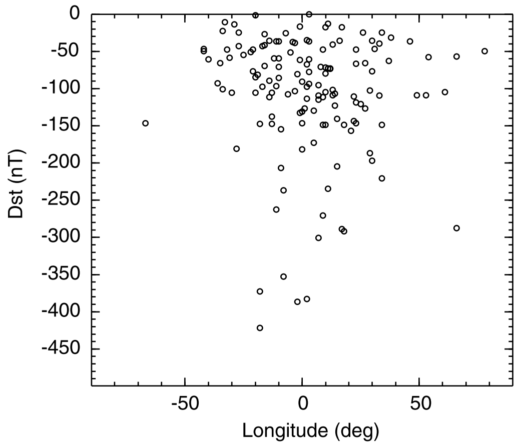

Figure 15 Minimum D_{st} plotted against ICME solar source longitude.

those ICMEs for which no source is identified. Overall, only 11% of ICMEs with no known source are associated with similar levels of geomagnetic activity.

4.11. Plasma Composition/Charge States

There is insufficient space to summarize of the behavior of the various SWICS solar wind ion composition and charge state parameters within our ICMEs, but a few points may be noted. Figure 16(a) shows the mean Fe ion charge state plotted against the intensity of the associated X-ray flare. Lepri and Zurbuchen (2004) suggest that flare heating is a primary cause of the enhanced ion charge states found in ICMEs. However, the mean iron charge state observations show no clear correlation with X-ray intensity with the exception of ICMEs associated with $>\approx$X3 flares, which only show strongly enhanced iron charge states (mean $\approx$15) that are among the highest found in this sample of ICMEs. The Mg/O ratio (Figure 16(b)) also shows enhanced values associated with the most intense ($>\approx$X3) flares, but a wide range of values for smaller flares, with no clear organization by flare intensity. In fact, the mean values of Mg/O and Q_{Fe}, and also $\mathrm{O}^7/\mathrm{O}^6$, are closely correlated in our sample of ICMEs, as illustrated in Figure 17. This correlation, relating the first ionization potential (FIP) effect and ion heating in ICMEs, was noted by Richardson and Cane (2004a). Although the "Mg/O" ratio has since been redefined in the revised SWICS data set to include a wider range of Mg ions, this relationship evidently still holds over a large sample of ICMEs.

5. Relationship between Plasma/Field, Compositional and Magnetic Cloud Boundaries

Figure 18 shows the distribution of the compositional/charge state boundary time offsets at the ICME leading (a) and trailing (b) edges, from Tables 1 to 12. Most frequently, there is close agreement between the ICME boundaries inferred from the plasma and magnetic field data and from the compositional/charge state data, consistent with the conclusion of Richardson and Cane (2004a) based on a summary of all the Cane and Richardson (2003) events (*cf.* their Figure 8). Of 210 events where the times of the leading edge of the ICME and compositional signatures can be compared, they are essentially simultaneous in 73%

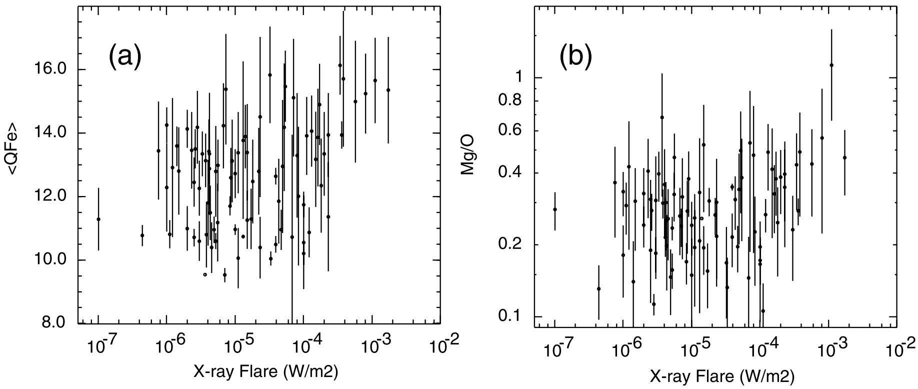

Figure 16 Variation of the solar wind mean Fe ion charge (a) and Mg/O ratio (b) with the X-ray intensity of the associated solar flare measured by GOES.

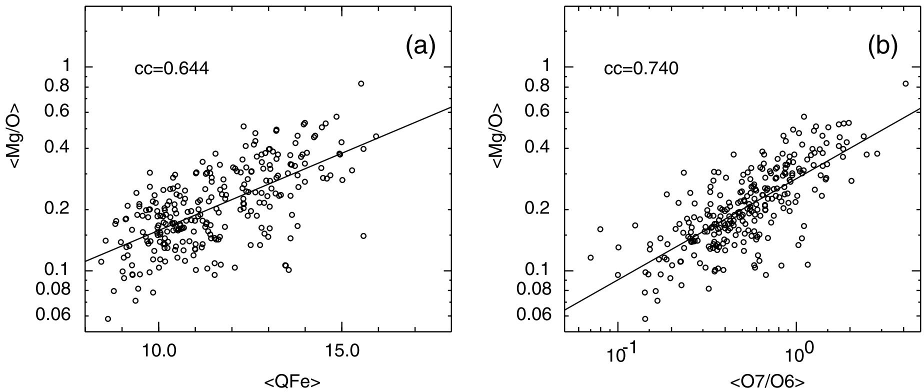

Figure 17 Correlation between mean Mg/O and the mean iron charge state (a) or O^7/O^6 ratio (b) in 267 and 268 ICMEs, respectively.

of these events. The mean time difference is +0.28 hour with a standard deviation of 5.64 hours. Considering events with time differences of at least 2 hours, there are 33 events (16% of all events) in which the compositional/charge state signature starts before the ICME leading edge, by an average of 6.6 hours (this may indicate the "true" arrival time of the ICME plasma), and 25 events (12%) in which the compositional signature starts after the ICME leading edge, by an average of 11.1 hours. At the ICME trailing edge, the mean time difference is +1.9 hours, and 116 out of 195 events (56%) have the trailing edges of the ICME and compositional signature co-located. In another 24 cases (12%), the compositional signature ends more than 2 hours inside the ICME trailing edge, with a mean time difference of 10.7 hours, while in 55 events (28%), the compositional/charge state signature extends more than 2 hours beyond the ICME, by a mean period of 11.4 hours. The implication of the latter result is that ICME-like plasma that was strongly heated near the Sun may be observed in the wake of the ICME as defined by other plasma and field signatures (*cf.* Figure 2; Gloeckler *et al.*, 1999).

Comparing ICME and magnetic cloud boundaries, in 52 out of 99 events (53%), there is close agreement between the ICME and MC leading edges (Figure 18(c)). Only one

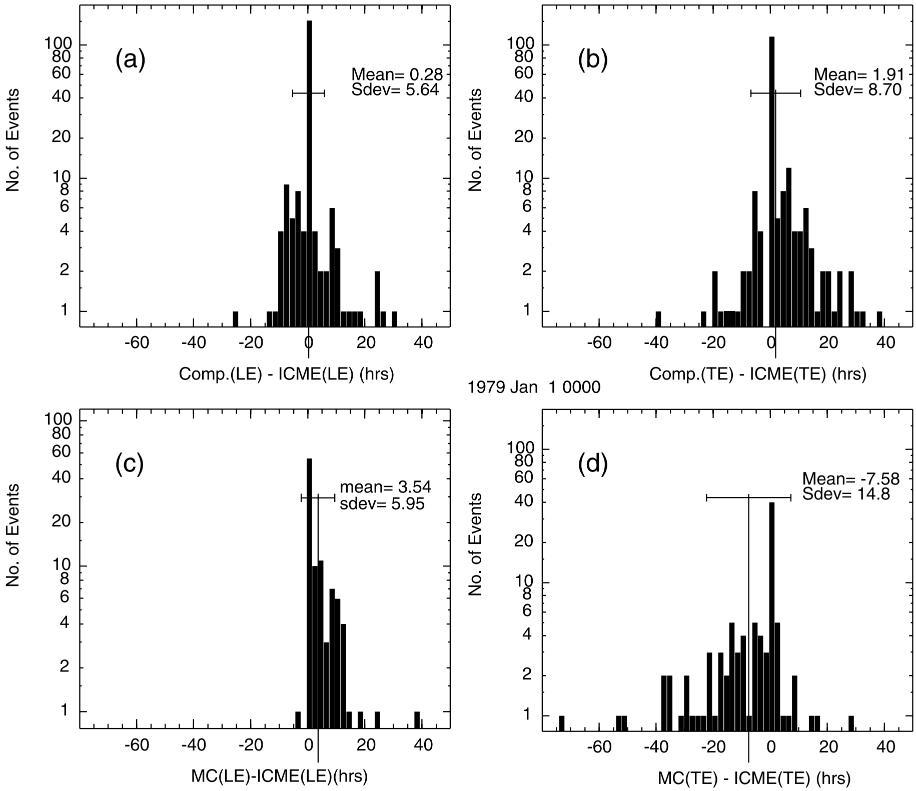

Figure 18 Histograms of the time differences between the leading and trailing edges of ICME-like compositional/charge state signatures ((a) and (b)) and magnetic clouds ((c) and (d)) with respect to the "plasma/magnetic field" boundaries given in Tables 1 to 12.

magnetic cloud (22 July 2004 on the WIND magnetic cloud list) commenced more than 2 hours ahead of our estimated ICME boundary, while there are 45 events in which the magnetic cloud leading edge is inside the ICME leading edge, with an average time offset of 8 ± 1.0 hours. At the trailing edge, 40 out of 98 events (41%) show general agreement between the ICME and magnetic cloud boundaries. Again there is an asymmetry in the distribution (Figure 18(d)), reflected in the mean time difference of -7.6 hours. Some 46 events (47%) have the magnetic cloud signature terminating at least 2 hours inside the ICME trailing edge, by a mean of 16.8 hours, while only 12 magnetic clouds terminate after the ICME trailing edge, by a mean of 8.3 hours. Overall, the reported MCs tend to start after and end earlier than the overall ICME boundaries we have identified in plasma/field data, as exemplified by the event in Figure 2. A reason for this pattern is that the reported magnetic cloud boundaries are usually defined by the start and end of a smooth rotation in field direction, because of the requirements of model fitting. Hence, they tend to define a substructure of the ICME that is identified without this requirement.

Figure 19 compares the ICME radial size and the time difference between the trailing edges of the ICME and magnetic cloud. The magnetic cloud and ICME trailing edge boundaries are in agreement only for ICMEs up to around 0.5 AU in size, while more extended ICMEs show an increasing time difference between the ICME and magnetic cloud trailing

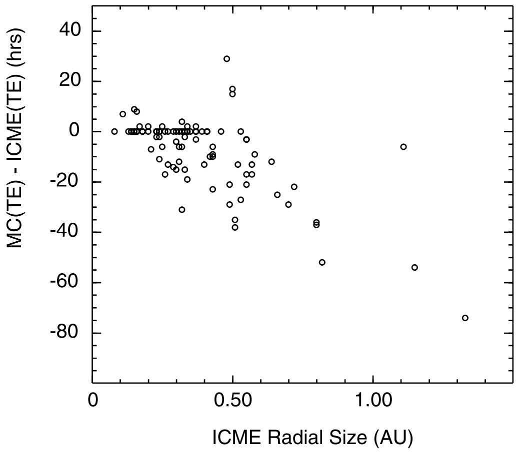

Figure 19 Time difference between ICME and magnetic cloud trailing edges plotted against the ICME radial size.

edges. The basic picture suggested by this figure is that the magnetic cloud is a substructure of the ICME that may be up to about 0.5 AU in size and is followed by a region of ICME-like material in more extended ICMEs.

6. Comparison with Other ICME Catalogs

In addition to Cane and Richardson (2003), several other near-Earth ICME catalogs for specific intervals during cycle 23 have been generated. Liu, Richardson, and Belcher (2005) produced an ICME catalog for 1995 – October 2002 using criteria based on abnormally low proton temperatures and a high He/proton ratio (>8%), a criterion that is only met in a subset of ICMEs (Richardson and Cane, 2004a). For the interval where our studies overlap, they identify 99 events, compared with our 217 events. They note that 85% of their events were in the Cane and Richardson (2003) catalog, as is also the case for our revised catalog. They also note that their ICME boundaries may differ significantly from Cane and Richardson (2003), a major factor being the greater importance placed on the He/p ratio. Examining the few Liu, Richardson, and Belcher (2005) events not in our catalog, we conclude that they may be possible ICMEs with weak signatures, or, in some cases, may be encounters with the heliospheric plasma sheet.

Russell and Shinde (2005) criticized the Cane and Richardson (2003) catalog by comparing it with several other published or unpublished ICME lists that, we note, emphasized the subset of ICMEs with magnetic cloud signatures and were not intended to be "comprehensive" event lists. They expressed concern at the much larger number of events identified by Cane and Richardson (2003), the relatively small number of events common to all these lists, events found on only one list, and ICME boundaries that differed between lists and when different ICME signatures are considered. We note though that criteria that select ICMEs with magnetic cloud-like features will inevitably miss a large fraction of ICMEs (*cf.* Figure 6). Furthermore, the differences in boundaries indicated by different ICMEs signatures, while potentially a problem for crisply defining the edges of ICMEs, presumably reflect the different physical processes involved in producing these signatures. It is not self-evident for example, that low *in-situ* solar wind proton temperatures (associated with ICME expansion in the solar wind), compositional and charge state signatures (imposed by conditions during CME release at the Sun), and bidirectional suprathermal electron flows (that depend on field line connectivity to the Sun) should occupy exactly the same regions of the solar wind at 1 AU. The inability in some cases to define ICME boundaries unambiguously should not be confused with an inability to identify ICMEs, especially when multiple signatures are present such as in the examples shown in this paper.

Such complexity also suggests that it is improbable a single parameter can indicate the "true" ICME interval, such as the total pressure (magnetic and plasma) perpendicular to the magnetic field proposed by Russell, Shinde, and Jian (2005) and Jian *et al.* (2006). Although Jian *et al.* (2006) emphasis the perpendicular pressure, and use it to develop a list of ICMEs in 1995 – 2004, they still refer to a number of more conventional ICME signatures, namely "the low proton temperature, a stronger than ambient magnetic field, a relatively quiet and smooth rotation in magnetic field, a helium abundance enhancement, and BDEs" when compiling their catalog. Jian *et al.* (2006) note that 82% of their events are in the Cane and Richardson (2003) catalog, and 67% of the Cane and Richardson (2003) events are in their catalog; similar results apply to our revised catalog. The differences lie mainly in: marginal events with weak ICME signatures that are included in one catalog and not the other (*e.g.*, 19 March 1999 in our catalog, 4 April 2000 in Jian *et al.* (2006)); events that may be heliospheric plasma sheet crossings rather than ICMEs that are included in one list and not the other (*e.g.*, 15 February 1996 in Jian *et al.* (2006)); events that have otherwise weak signatures but are prominent in composition/charge state data and are included in our list (*e.g.*, 26 November 2000); shock sheaths that are not followed by clear ICME signatures but are nevertheless included by Jian *et al.* (2006) (*e.g.*, 13 and 31 January 2001; 25 and 29 July, 26 August, 26 November, 2002); and clear events in our list that are missing from Jian *et al.* (2006) for some reason (*e.g.*, 11 October 2001; 7 November 2004). Jian *et al.* (2006) interpret the perpendicular pressure – time profiles in terms of the spacecraft trajectory relative to a magnetic obstacle, assumed to be a magnetic flux rope. However, this scenario appears to be inadequate to incorporate the clear presence of ICME-like plasma without flux-rope-like magnetic fields in many events. In particular, the lack of a flux-rope signature does not appear to suggest just a "glancing" encounter with the ICME.

Schwenn *et al.* (2005) have summarized the properties of "ICME events" identified between 1997 and April 2001. They use a rather broad definition of an ICME, including the passage of shocks (that are not necessarily followed by an ICME encounter), geomagnetic storms with $D_{st} < -50$ nT (which, however, may be associated with other solar wind features such as corotating interaction regions; Richardson *et al.*, 2006), magnetic clouds, and "plasma (density) blobs". Schwenn *et al.* (2005) state that comparing their list with Cane and Richardson (2003) is "a mess". However, we believe this is a pessimistic assessment: We estimate that 56% of the Schwenn *et al.* (2005) events are associated with Cane and Richardson (2003) events – we would certainly only call this a fair agreement. On the other hand, examining the plasma/field/compositional signatures, we suggest that 46 of the Schwenn *et al.* (2005) "ICMEs" (21%) are corotating interaction regions compared with their estimate of only 4%. Another 25 events show no evidence of ICME-like plasma/field signatures following a shock, and would not appear on our list. A further three events have ACE data gaps and we did not classify these in Cane and Richardson (2003). Removing these events, then the association rate is ≈84%. Thus, we suggest that there is a reasonably good agreement between the Schwenn *et al.* (2005) and Cane and Richardson (2003) events (and with the current list) once the CIR and shock events without ICMEs are removed from the Schwenn *et al.* (2005) list. The remaining differences between the lists lie in events that do not have the signatures examined by Schwenn *et al.* (2005), but otherwise have reasonably clear ICME signatures, and events with marginal ICME signatures.

7. Summary and Conclusions

We have cataloged the over 300 ICMEs that were observed in the near-Earth solar wind in 1996 – 2009, encompassing solar cycle 23, and summarized their properties. Our conclusions include:

- The ICME rate broadly follows solar activity levels, increasing by around an order of magnitude from solar minimum to solar maximum. However, the rate/solar rotation is relatively constant over much of the cycle at $\approx$2 – 3 ICMEs/rotation, but punctuated by short increases associated with the presence of major active regions on the Sun. Wavelet analysis of the ICME rate shows evidence of intermittent periodicities of $\approx$160 days near solar maximum and $\approx$130 days during the late declining phase.
- Observations for 2009 show an upturn in the ICME rate, apparently related to the onset of cycle 24, following two years with few ICMEs.
- Average properties of our ICMEs are in close agreement with those obtained in other studies, including those using events from previous solar cycles.
- Though the magnetic cloud fraction has increased during previous solar minima, few clear magnetic clouds have been observed during the extended minimum at the end of cycle 23. The fraction of ICMEs that are magnetic clouds may increase for ICMEs with source regions at $\approx$0 to 20°W.
- Taken as a group, our ICMEs do not appear to follow the dimensionless expansion demonstrated by Démoulin *et al.* (2008), Démoulin (2010) and Gulisano *et al.* (2010) for selected groups of magnetic clouds.
- The level of geomagnetic activity produced by an ICME or the associated sheath (as measured by D_{st}) is highly correlated with the maximum 1-hour averaged value of B_{s} or E_y, but not with the ICME speed. For a >50% probability of an ICME/sheath producing an intense storm ($D_{\mathrm{st}} \le -100$ nT), $E_y > 6\ \mathrm{mV\,m^{-1}}$ is required.
- The extensively studied flux-rope-like "magnetic cloud" structures are occasionally only substructures of larger regions of ICME-like plasma indicated by solar wind plasma, magnetic field, composition and charge state data. Thus, plasma that has been processed and heated near the Sun is not confined to the flux-rope structure that may be present. Observations of ICME-like plasma regions with radial sizes >0.5 AU suggest that extended outflows of heated plasma may occur and/or multiple ICMEs may contribute.
- Individual ICMEs may exhibit a number of characteristic signatures formed by various independent processes at the Sun and in the solar wind, and the "ICME boundaries" inferred from these signatures frequently differ. It is therefore unlikely that a single parameter can be identified that indicates the "true" ICME boundaries.

Acknowledgements We are indebted to all the experimenters who have produced and generously made available the various data sets used to compile this catalog. The LASCO CME catalog is generated and maintained at the CDAW Data Center by NASA and The Catholic University of America in cooperation with the Naval Research Laboratory. SOHO is a project of international cooperation between ESA and NASA. This work was funded by a NASA Heliosphysics Guest Investigator award.

References

Aellig, M.R., Lazarus, A.J., Steinberg, J.T.: 2001, *Geophys. Res. Lett.* **28**, 2767.
Bochsler, P.: 2000, *Rev. Geophys.* **38**, 247.
Bothmer, V., Schwenn, R.: 1998, *Ann. Geophys.* **16**, 1.
Borrini, G., Gosling, J.T., Bame, S.J., Feldman, W.C.: 1982, *J. Geophys. Res.* **87**, 7370.

Burlaga, L.F., Plunkett, S.P., St. Cyr, O.C.: 2002, *J. Geophys. Res.* **107**, 1266.
Burlaga, L., Fitzenreiter, R., Lepping, R., Ogilvie, K., Szabo, A., Lazarus, A., *et al.*: 1998, *J. Geophys. Res.* **103**, 227.
Burlaga, L.F., Skoug, R.M., Smith, C.W., Webb, D.F., Zurbuchen, T.H., Reinard, A.: 2001, *J. Geophys. Res.* **106**, 20957.
Cane, H.V.: 1988, *J. Geophys. Res.* **93**, 1.
Cane, H.V.: 2000, *Space Sci. Rev.* **93**, 55.
Cane, H.V., Lario, D.: 2006, *Space Sci. Rev.* **123**, 45.
Cane, H.V., Richardson, I.G.: 2003, *J. Geophys. Res.* **108**(A4), SSH6-1.
Cane, H.V., Reames, D.V., von Rosenvinge, T.T.: 1988, *J. Geophys. Res.* **93**, 9555.
Cane, H.V., Richardson, I.G., St. Cyr, O.C.: 2000, *Geophys. Res. Lett.* **27**, 3591.
Cane, H.V., Richardson, I.G., von Rosenvinge, T.T.: 2010, *J. Geophys. Res.* doi:10.1029/2009JA014848.
Cane, H.V., Erickson, W.C., Prestage, N.P.: 2002, *J. Geophys. Res.* **107**(A10), SSH14-1.
Cane, H.V., Richardson, I.G., von Rosenvinge, T.T., Wibberenz, G.: 1994, *J. Geophys. Res.* **99**, 21429.
Cane, H.V., Mewaldt, R.A., Cohen, C.M.S., von Rosenvinge, T.T.: 2006, *J. Geophys. Res.* **111**, A06S90.
Dasso, S., Mandrini, C.H., Schmieder, B., Cremades, H., Cid, C., Cerrato, Y., *et al.*: 2009, *J. Geophys. Res.* **114**, A02109.
Démoulin, P.: 2010, In: Maksimovic, M., Issautier, K., Meyer-Vernet, N., Moncuquet, M., Pantellini, F. (eds.) *Twelfth International Solar Wind Conference*, *AIP Conf. Proc.* **1216**, 329.
Démoulin, P., Nakwacki, M.S., Dasso, S., Mandrini, C.H.: 2008, *Solar Phys.* **250**, 347.
Dimitropoulou, M., Moussas, X., Strintzi, D.: 2008, *Mon. Not. Roy. Astron. Soc.* **386**, 2278.
Echer, E., Gonzalez, W.D., Tsurutani, B.T., Gonzalez, A.L.C.: 2008, *J. Geophys. Res.* **113**, A05221.
Forsyth, R.J., Bothmer, V., Cid, C., Crooker, N.U., Horbury, T.S., Kecskemety, K., *et al.*: 2006, *Space Sci. Rev.* **123**, 383.
Gloeckler, G., Cain, J., Ipavich, F.M., Tums, E.O., Bedini, P., Fisk, L.A., *et al.*: 1998, *Space Sci. Rev.* **86**, 497.
Gloeckler, G., Fisk, L.A., Hefti, S., Schwadron, N.A., Zurbuchen, T.H., Ipavich, F.M., Geiss, J., Bochsler, P., Wimmer-Schweingruber, R.F.: 1999, *Geophys. Res. Lett.* **26**, 157.
Gopalswamy, N.: 2006, *Space Sci. Rev.* **124**, 145.
Gopalswamy, N., Lara, A., Lepping, R.P., Kaiser, M.L., Berdichevsky, D., St. Cyr, O.C.: 2000, *Geophys. Res. Lett.* **27**, 145.
Gopalswamy, N., Lara, A., Yashiro, S., Kaiser, M.L., Howard, R.A.: 2001, *J. Geophys. Res.* **106**, 29207.
Gosling, J.T.: 1990, In: Russell, C. T., Priest, E. R., Lee, L. C. (eds.) *Physics of Magnetic Flux Ropes, AGU Geophys. Monogr.* **58**, 343.
Gosling, J.T.: 2000, In: Dingus, B. L., Kieda, D., Salamon, M. (eds.) *Proc. 26th Int. Cosmic Ray Conf.*, *AIP Conf. Proc.* **516**, 59.
Gosling, J.T., Pizzo, V., Bame, S.J.: 1973, *J. Geophys. Res.* **78**, 2001.
Gosling, J.T., Asbridge, J.R., Bame, S.J., Feldman, W.C., Zwickl, R.D.: 1980, *J. Geophys. Res.* **85**, 3431.
Gosling, J.T., Baker, D.N., Bame, S.J., Feldman, W.C., Zwickl, R.D., Smith, E.J.: 1987a, *J. Geophys. Res.* **92**, 8519.
Gosling, J.T., Thomsen, M.F., Bame, S.J., Zwickl, R.D.: 1987b, *J. Geophys. Res.* **92**, 12399.
Gulisano, A.M., Démoulin, P., Dasso, S., Ruiz, M.E., Marsch, E.: 2010, *Astron. Astrophys.* **509**, A39.
Hirshberg, J., Bame, S.J., Robbins, D.E.: 1972, *Solar Phys.* **23**, 467.
Hundhausen, A.J., Gilbert, H.E., Bame, S.J.: 1968, *J. Geophys. Res.* **73**, 5485.
Huttunen, K.E.J., Schwenn, R., Bothmer, V., Koskinen, H.E.J.: 2005, *Ann. Geophys.* **23**, 625.
Jian, L., Russell, C.T., Luhmann, J.G., Skoug, R.M.: 2006, *Solar Phys.* **239**, 393.
Kasper, J., Stevens, M.L., Lazarus, A.J., Steinberg, J.T., Ogilvie, K.W.: 2007, *Astrophys. J.* **660**, 901.
Klecker, B., Kunow, H., Cane, H.V., Dalla, S., Heber, B., Kecskemety, K., *et al.*: 2006, *Space Sci. Rev.* **123**, 217.
Klein, L.W., Burlaga, L.F.: 1982, *J. Geophys. Res.* **87**, 613.
Lean, J.L.: 1990, *Astrophys. J.* **363**, 718.
Leitner, M., Farrugia, C.J., Möstl, C., Ogilvie, K.W., Galvin, A.B., Schwenn, R., Biernat, H.K.: 2007, *J. Geophys. Res.* **112**, A06113.
Lepri, S.T., Zurbuchen, T.H.: 2004, *J. Geophys. Res.* **109**, A01112.
Lepri, S.T., Zurbuchen, T.H., Fisk, L.A., Richardson, I.G., Cane, H.V., Gloeckler, G.: 2001, *J. Geophys. Res.* **106**, 29231.
Liu, Y., Richardson, J.D., Belcher, J.W.: 2005, *Planet. Space Sci.* **53**, 3.
Liu, C., Lee, J., Yurchyshyn, V., Deng, N., Cho, K., Karlický, M., Wang, H.: 2007, *Astrophys. J.* **669**, 1372.
Lou, Y.Q.: 2000, *Astrophys. J* **540**, 1102.
Malandraki, O.E., Lario, D., Lanzerotti, L.J., Sarris, E.T., Geranios, A., Tsiropoula, G.: 2005, *J. Geophys. Res.* **110**, A09S06.
McGuire, R.E., von Rosenvinge, T.T., McDonald, F.B.: 1986, *Astrophys. J.* **301**, 938.

Michalek, G., Gopalswamy, N., Lara, A., Manoharan, P.K.: 2004, *Astron. Astrophys.* **423**, 729.
Neugebauer, M., Goldstein, R.: 1997, In: Crooker, N., Joselyn, J.A., Feynman, J. (eds.) *Coronal Mass Ejections, AGU Geophys. Monogr.* **99**, 245.
Neugebauer, M., Goldstein, R., Goldstein, B.E.: 1997, *J. Geophys. Res.* **102**, 19743.
Owens, M.J., Cargill, P.J., Pagel, C., Siscoe, G.L., Crooker, N.U.: 2005, *J. Geophys. Res.* **110**, A01105.
Owocki, S.P., Holzer, T.E., Hundhausen, A.J.: 1983, *Astrophys. J.* **275**, 354.
Rakowski, C., Laming, J.M., Lepri, S.T.: 2007, *Astrophys. J.* **667**, 602.
Reinard, A.: 2005, *Astrophys. J.* **620**, 501.
Reinard, A.: 2008, *Astrophys. J.* **682**, 1289.
Reinard, A.A., Zurbuchen, T.H., Fisk, L.A., Lepri, S.T., Skoug, R.M., Gloeckler, G.: 2001, In: Wimmer-Schweingruber, R.F. (ed.) *Solar and Galactic Composition*, *AIP Conf. Proc.* **598**, 139.
Reisenfeld, D.B., Steinberg, J.T., Barraclough, B.L., Dors, E.E., Wiens, R.C., Neugebauer, M., Reinard, A., Zurbuchen, T.: 2003, In: Velli, M., Bruno, R., Malara, F. (eds.) *Solar Wind Ten, AIP Conf. Proc.* **679**, 632.
Reisenfeld, D.B., Burnett, D.S., Becker, R.H., Grimberg, A.G., Heber, V.S., Hohenberg, C.M., *et al.*: 2007, *Space Sci. Rev.* **130**, 79.
Richardson, I.G.: 1994, *Astrophys. J.* **420**, 926.
Richardson, I.G.: 2004, *Space Sci. Rev.* **111**, 267.
Richardson, I.G., Cane, H.V.: 1993, *J. Geophys. Res.* **98**, 15295.
Richardson, I.G., Cane, H.V.: 1995, *J. Geophys. Res.* **100**, 23397.
Richardson, I.G., Cane, H.V.: 1996, *J. Geophys. Res.* **101**, 27521.
Richardson, I.G., Cane, H.V.: 2004a, *J. Geophys. Res.* **109**, A09104.
Richardson, I.G., Cane, H.V.: 2004b, *Geophys. Res. Lett.* **31**, L18804.
Richardson, I.G., Cane, H.V.: 2005a, *Geophys. Res. Lett.* **32**, L02104.
Richardson, I.G., Cane, H.V.: 2005b, In: Fleck, B., Zurbuchen, T.H., Lacoste, H. (eds.) *Proceedings of Solar Wind 11/SOHO 16, Connecting Sun and Heliosphere, ESA SP-592*, 755.
Richardson, I.G., Cane, H.V.: 2010, In: Maksimovic, M., Issautier, K., Meyer-Vernet, N., Moncuquet, M., Pantellini, F. (eds.) *Twelfth International Solar Wind Conference*, *AIP Conf. Proc.* **1216**, 683.
Richardson, I.G., Reames, D.V.: 1993, *Astrophys. J. Suppl.* **85**, 411.
Richardson, I.G., Zhang, J.: 2008, *Geophys. Res. Lett.* **35**, L06S07.
Richardson, I.G., Cane, H.V., Wibberenz, G.: 1999, *J. Geophys. Res.* **104**, 12549.
Richardson, I.G., Berdichevsky, D., Desch, M.D., Farrugia, C.J.: 2000, *Geophys. Res. Lett.* **27**, 3761.
Richardson, I.G., Cane, H.V., Lepri, S.T., Zurbuchen, T.H., Gosling, J.T.: 2003a, In: Velli, M., Bruno, R., Malara, F. (eds.) *Solar Wind Ten, AIP Conf. Proc.* **679**, 681.
Richardson, J.D., Richardson, I.G., Kasper, J.C., Cane, H.V., Crooker, N.U., Lazarus, A.J.: 2003b, In: Wilson, A. (ed.) *Solar Variability as an Input to the Earth's Environment, International Solar Cycle Studies (ISCS) Symposium, ESA SP-535*, 521.
Richardson, I.G., Webb, D.F., Zhang, J., Berdichevsky, D.B., Biesecker, D.A., Kasper, J.C., *et al.*: 2006, *J. Geophys. Res.* **111**, A07S09.
Rieger, E., Share, G.H., Forrest, D.J., Kanbach, G., Reppin, C., Chupp, E.L.: 1984, *Nature* **312**, 623.
Russell, C.T., Shinde, A.A.: 2005, *Solar Phys.* **229**, 323.
Russell, C.T., Shinde, A.A., Jian, L.: 2005, *Adv. Space Res.* **35**, 2178.
Sanderson, T.R., Beeck, J., Marsden, R.G., Tranquille, C., Wenzel, K.-P., McKibben, R.B., Smith, E.J.: 1990, In: *Proc. 21st Int. Cosmic Ray Conf.* **6**, 251.
Schwenn, R., Rosenbauer, H., Muehlhaeuser, K.-H.: 1980, *Geophys. Res. Lett.* **7**, 201.
Schwenn, R., Lago, A. Dal, Huttunen, E., Gonzalez, W.D.: 2005, *Ann. Geophys.* **23**, 1033.
Shodhan, S., Crooker, N.U., Kahler, S.W., Fitzenreiter, R.J., Larson, D.E., Lepping, R.P., Siscoe, G.L., Gosling, J.T.: 2000, *J. Geophys. Res.* **105**, 27261.
Skoug, R.M., Bame, S.J., Feldman, W.C., Gosling, J.T., McComas, D.J., Steinberg, J.T., *et al.*: 1999, *Geophys. Res. Lett.* **26**, 161.
Torrence, C., Compo, G.P.: 1998, *Bull. Am. Meteor. Soc.* **79**, 61.
Vršnak, B., Gopalswamy, N.: 2002, *J. Geophys. Res.* **107**(A2), SSH2-1.
Wang, C., Du, D., Richardson, J.D.: 2005, *J. Geophys. Res.* **110**, A10107.
Wang, Y.M., Ye, P.Z., Wang, S., Zhou, G.P., Wang, J.X.: 2002, *J. Geophys. Res.* **107**, 1340.
Wibberenz, G., Richardson, I.G., Cane, H.V.: 2002, *J. Geophys. Res.* **107**(A11), SSH5-1.
Wu, C.-C., Lepping, R.P.: 2007, *Solar Phys.* **242**, 159.
Yermolaev, Yu.I., Zhuravlev, V.I., Zastenker, G.N., Kogan, V.T., Koshevenko, B.V., Pavlov, A.K., Soboleva, E.V., Chichagov, Yu.V.: 1989, *Cosm. Res.* **27**, 614.
Yurchyshyn, V., Liu, C., Abramenko, V., Krall, J.: 2006, *Solar Phys.* **239**, 317.
Zaqarashvili, T.V., Carbonell, M., Oliver, R., Ballester, J.L.: 2010, *Astrophys. J.* **709**, 749.
Zhang, J., Richardson, I.G., Webb, D.F.: 2008, *J. Geophys. Res.* **113**, A00A12.

Zhang, J., Poomvises, W., Richardson, I.G.: 2008, *Geophys. Res. Lett.* **35**, L02109.
Zhang, J., Richardson, I.G., Webb, D.F., Gopalswamy, N., Huttunen, E., Kasper, J., *et al.*: 2007, *J. Geophys. Res.* **112**, A10102.
Zurbuchen, T.H., Richardson, I.G.: 2006, *Space Sci. Rev.* **123**, 31.
Zurbuchen, T.H., Fisk, L.A., Lepri, S.T., von Steiger, R.: 2003, In: Velli, M., Bruno, R., Malara, F. (eds.) *Solar Wind Ten, AIP Conf. Proc.* **679**, 604.
Zwickl, R.D., Asbridge, J.R., Bame, S.J., Feldman, W.C., Gosling, J.T.: 1982, *J. Geophys. Res.* **87**, 7379.
Zwickl, R.D., Asbridge, J.R., Bame, S.J., Feldman, W.C., Gosling, J.T., Smith, E.J.: 1983, In: Neugebauer, M. (ed.) *Solar Wind Five*, *ASP Conf. Ser.* **2280**, 711.